Nonperturbative renormalization of composite operators with overlap fermions

J. B. Zhang,[1,2] N. Mathur,[3,4] S. J. Dong,[3] T. Draper,[3] I. Horváth,[3] F. X. Lee,[5] D. B. Leinweber,[2] K. F. Liu,[3] and A. G. Williams[2]

[1]*Zhejiang Institute of Modern Physics and Department of Physics, Zhejiang University, Hangzhou 310027, People's Republic of China*
[2]*Special Research Center for the Subatomic Structure of Matter and Department of Physics, University of Adelaide, Adelaide, SA 5005, Australia*
[3]*Department of Physics and Astronomy, University of Kentucky, Lexington, Kentucky 40506, USA*
[4]*Jefferson Lab, 12000 Jefferson Avenue, Newport News, Virginia 23606, USA*
[5]*Center for Nuclear Studies, Department of Physics, George Washington University, Washington, D.C. 20052, USA*

(Received 3 August 2005; published 20 December 2005)

We compute nonperturbatively the renormalization constants of composite operators on a quenched $16^3 \times 28$ lattice with lattice spacing $a = 0.20$ fm for the overlap fermion by using the regularization-independent (RI) scheme. The quenched gauge configurations were generated with the Iwasaki action. We test the relations $Z_A = Z_V$ and $Z_S = Z_P$ and find that they agree well (less than 1%) above $\mu = 1.6$ GeV. We also perform a Renormalization Group (RG) analysis at the next-to-next-to-leading order and match the renormalization constants to the $\overline{\text{MS}}$ scheme. The wave function renormalization Z_ψ is determined from the vertex function of the axial current and Z_A from the chiral Ward identity. Finally, we examine the finite quark mass behavior for the renormalization factors of the quark bilinear operators. We find that the $(pa)^2$ errors of the vertex functions are small and the quark mass dependence of the renormalization factors to be quite weak.

DOI: 10.1103/PhysRevD.72.114509 PACS numbers: 12.38.Gc, 11.15.Ha, 12.38.Aw

I. INTRODUCTION

Lattice QCD is a unique tool to compute the mass spectrum, leptonic decay constants and hadronic matrix elements of local operators nonperturbatively from first principles. Renormalization of lattice operators is an essential ingredient needed to deduce physical results from numerical simulations. In this paper we study the renormalization properties of composite bilinear operators with the overlap quark action.

In principle, renormalization of quark bilinears can be computed by lattice perturbation theory. However, it is generally difficult to go beyond one loop in such calculations. To overcome these difficulties, Martinelli *et al.* [1] have proposed a promising nonperturbative renormalization procedure. The procedure allows a full nonperturbative computation of the matrix elements of composite operators in the regularization-independent (RI) scheme [1,2]. The matching between the RI scheme and $\overline{\text{MS}}$, which is intrinsically perturbative, is computed using only the well behaved continuum perturbation theory.

This method has been shown to be quite successful in reproducing results obtained by other methods, such as chiral Ward Identities [3]. The method has also been successfully applied to determine renormalization coefficients for various operators using the Wilson [4–7], staggered [8], domain-wall [9], chirally improved [10], and overlap fermions [11,12]. The purpose of the current work is to study the application of this nonperturbative renormalization procedure to the renormalization of the quark field and the flavor nonsinglet fermion bilinear operators, and also to study their quark mass dependence for the case of overlap fermions.

Neuberger's overlap fermion [13,14] is shown to have correct anomaly and exact chiral symmetry on the lattice [13–15] with finite cutoff. As a consequence, many chiral-symmetry relations [15,16] and the quark propagator [17] preserve the same structure as in the continuum. The use of the overlap action entails many theoretical advantages [18]: it has no additive mass renormalization, there are no $O(a)$ artifacts, and it has good scaling behavior with small $O(a^2)$ and $O(m^2a^2)$ errors [17,19]. In addition, it forbids mixing among operators of different chirality and, therefore, can be very helpful in computing weak matrix elements.

The outline of this paper is as follows. In Sec. II, we review the nonperturbative method (NPM) proposed in Ref. [1] and introduce the notation used in the remainder of this work. In Sec. III, we briefly describe the overlap fermion formalism. We present the numerical results for the renormalization constants as well as the Renormalization Group (RG) analysis of the quark bilinear in Sec. IV and Sec. V. In Sec. VI, we examine the finite m behavior of the renormalization factors of the quark bilinear operators. We complete our discussion with our conclusions in Sec. VII.

II. NONPERTURBATIVE RENORMALIZATION METHOD

In this section, we review the nonperturbative renormalization method of Ref. [1], which we will use to compute the renormalization constants of quark bilinears in this paper. The method imposes renormalization conditions nonperturbatively, directly on quark and gluon Green's functions in Landau gauge.

We start by considering the definition for the momentum space quark propagator. Let $S(x, 0)$ be the quark propagator on the gauge-fixed configuration from a source 0 to all space-time points x. The momentum space propagator is defined as the discrete Fourier transform over the sink positions

$$S(p, 0) = \sum_x \exp(-ip^{\text{latt}} \cdot x) S(x, 0), \tag{1}$$

where p^{latt} is the dimensionless lattice momenta.

In our case, we use the periodic boundary condition in spatial directions and the antiperiodic boundary condition in time direction. We have then the dimensionful momenta

$$\begin{aligned} p_i &= \frac{2\pi}{N_s a}(n_i - N_i/2), \quad \text{and} \\ p_t &= \frac{2\pi}{N_t a}(n_t - 1/2 - N_t/2), \end{aligned} \tag{2}$$

for an $N_s^3 \times N_t$ lattice.

We also define the square of the absolute momentum as the Euclidean inner product of the momenta defined in Eq. (2)

$$(pa)^2 = \sum_\mu p_\mu^{\text{latt}} p_\mu^{\text{latt}}, \tag{3}$$

where we use convention that p is dimensionful and p_μ^{latt} is dimensionless.

A. Three-Point Function

Consider the flavor nonsinglet fermion bilinear operator

$$O_\Gamma(x) = \bar{\psi}(x)\Gamma\psi(x), \tag{4}$$

where Γ is the Dirac gamma matrix

$$\Gamma \in \{1, \gamma_\mu, \gamma_5, \gamma_\mu\gamma_5, \sigma_{\mu\nu}\}, \tag{5}$$

and the corresponding notation will be {S, V, P, A, T}, respectively. The flavor index is suppressed. The connected three-point function with an operator insertion at position 0 between the quark fields at x and y is given by

$$G_O(x, 0, y) = \langle \psi(x) O_\Gamma(0) \bar{\psi}(y) \rangle = \langle S(x, 0)\Gamma S(0, y) \rangle, \tag{6}$$

where $S(0, y)$ is the quark propagator from y to 0. It is the inverse of the Dirac operator.[1] Note, $S(x, 0)$ here is not translational invariant. Only when averaging over all gauge configurations, i.e.,

$$\langle S(x, 0) \rangle, \tag{7}$$

is it translational invariant.

[1]Note that since we use the overlap fermion formalism, the fermion field ψ in Eqs. (4) and (6) will be replaced by $\hat{\psi} = (1 - D/2)\psi$, where D is the massless overlap operator. As a result, the $S(x, 0)$ and $S(0, y)$ are effective quark propagators to be described in Sec. III.

Using γ_5 Hermiticity, the Fourier transform of the three-point function is given by

$$\begin{aligned} G_O(pa, p'a) &\equiv \int d^4x d^4y e^{-i(p\cdot x - p'\cdot y)} G_O(x, 0, y), \\ &= \left\langle \left(\int d^4x S(x, 0) e^{-ip\cdot x} \right) \right. \\ &\quad \left. \times \Gamma \left(\int d^4y S(0, y) e^{ip'\cdot y} \right) \right\rangle, \\ &= \left\langle S(p, 0)\Gamma\gamma_5 \left(\int d^4y S^\dagger(y, 0) e^{ip'\cdot y} \right) \gamma_5 \right\rangle, \end{aligned} \tag{8}$$

where the † refers only to the color and spin indices. This can be written as

$$G_O(pa, p'a) = \langle S(p, 0)\Gamma(\gamma_5 S^\dagger(p', 0)\gamma_5) \rangle. \tag{9}$$

From this, one can define the vertex function as the amputated three-point function

$$\Lambda_O(pa, p'a) = S(pa)^{-1} G_O(pa, p'a) S(p'a)^{-1}, \tag{10}$$

where

$$S(pa) = \langle S(p, 0) \rangle, \tag{11}$$

which is translational invariant and is a 12×12 matrix in color-spin space.

Finally, a projected vertex function is defined

$$\Gamma_O(pa) = \frac{1}{\text{Tr}(\hat{P}_O^2)} \text{Tr}(\Lambda_O(pa, pa)\hat{P}_O), \tag{12}$$

where $\hat{P}_O = \Gamma$ is the corresponding projection operator.

B. RI-MOM Renormalization Condition

The renormalized operator $O(\mu)$ is related to the bare operator

$$O(\mu) = Z_O(\mu a, g(a)) O(a), \tag{13}$$

and the renormalization condition is imposed on the three-point vertex function $\Gamma_O(pa)$ at a scale $p^2 = \mu^2$ as

$$\Gamma_{O,\text{ren}}(pa)|_{p^2=\mu^2} = \frac{Z_O(\mu a, g(a))}{Z_\psi(\mu a, g(a))} \Gamma_O(pa)|_{p^2=\mu^2} = 1 \tag{14}$$

to make it agree with the tree-level value of unity [1]. The procedure is often called RI-MOM scheme, in which MOM means momentum scheme, it is also simply called RI scheme. Here Z_ψ is the field or wave function renormalization

$$\psi_{\text{ren}} = Z_\psi^{1/2} \psi. \tag{15}$$

In order to alleviate the nonperturbative effects from the spontaneous chiral-symmetry breaking, high virtuality with $\mu \gg \Lambda_{\text{QCD}}$ is required. On the other hand, to avoid the discretization errors, one would need $\mu \ll 1/a$. So, for the RI-MOM procedure to be a valid and practical renormalization scheme, there should exist a window in the

renormalization scale μ, i.e. $\Lambda_{\rm QCD} \ll \mu \ll 1/a$. In this work, the renormalization constants are extracted from $(pa)^2 > 1$ which, in principle, should have large discretization errors. But, as we will see later, we do not see large discretization errors. This is also the case observed in previous studies [1,4,9,12].

In practice, one usually matches the results to the perturbative scheme, e.g. $\overline{\rm MS}$ scheme, in order to compare with experimental quantities. We will discuss perturbative matching in Sec. IV. In general, the vertex function $\Gamma_O(pa)$ may have intrinsically nonperturbative contributions, e.g. from the Goldstone boson propagator, which are not included in perturbative calculations. To this end, we either go to large enough momentum such that the nonperturbative effects are suppressed or somehow remove them from the data.

There are several ways to obtain the renormalization constant Z_O for the operator O. For the Z_ψ in Eq. (14), one could use a known ratio involving Z_ψ to have it eliminated in Eq. (14). The first way is to extract Z_ψ from the vertex function of the conserved vector or axial-vector current. For example, if one uses the conserved vector current, then $Z_{V_C} = 1$. From the renormalization condition

$$\frac{Z_{V_C}}{Z_\psi}\Gamma_{V_C}(pa)|_{p^2=\mu^2} = 1, \tag{16}$$

one then obtains

$$Z_\psi = \frac{1}{48}\mathrm{Tr}(\Lambda_{V_{C\mu}}(pa)\gamma_\mu)|_{p^2=\mu^2}. \tag{17}$$

One can also extract Z_ψ directly from the quark propagator. From Ward Identity (WI), it follows [1]

$$Z_\psi = \frac{-i}{12}\mathrm{Tr}\Big[\frac{\partial S(pa)^{-1}}{\partial p}\Big]_{p^2=\mu^2}. \tag{18}$$

To avoid derivatives with respect to a discrete variable, it is suggested [1] to use

$$Z'_\psi = \frac{-i}{12}\frac{\mathrm{Tr}\sum_{\mu=1}^4 \gamma_\mu(p_\mu a)S(pa)^{-1}}{4\sum_{\mu=1}^4(p_\mu a)^2}\Bigg|_{p^2=\mu^2}, \tag{19}$$

which, in the Landau gauge, differs from Z_ψ by a finite term of order α_s^2 [20]. The matching coefficient can be computed using continuum perturbation theory, and up to order α_s^2 [20]

$$\frac{Z'_\psi}{Z_\psi} = 1 - \frac{\alpha_s^2}{(4\pi)^2}\Delta_\psi^{(2)} + \ldots. \tag{20}$$

In the Landau gauge

$$\Delta_\psi^{(2)} = \frac{(N_c^2-1)}{16N_c^2}(3 + 22N_c^2 - 4N_c n_f), \tag{21}$$

where N_c is the number of colors and n_f the number of dynamical quarks. However, as pointed out in Ref. [9], due to the ambiguity as to how the discrete lattice momentum p is defined, this method will introduce roughly 10%–20% uncertainty in determining Z_ψ.

The third way is to first calculate the renormalization constant Z_A from the axial Ward identity [11,19,21] with a local current, and then use the renormalization condition for the axial current

$$\frac{Z_A}{Z_\psi}\Gamma_A(pa)|_{p^2=\mu^2} = 1, \tag{22}$$

to eliminate the unknown Z_ψ from Eq. (14). Combining Eqs. (14), (22), and the Z_A from the Ward identity, one obtains

$$Z_O = Z_A\frac{\Gamma_A(pa)|_{p^2=\mu^2}}{\Gamma_O(pa)|_{p^2=\mu^2}}. \tag{23}$$

This way, other renormalization constants, such as Z_S, Z_P, Z_V, and Z_T can be obtained and the identity relations $Z_S = Z_P$ and $Z_V = Z_A$ due to chiral symmetry can be checked. Note here, the local axial-vector current is finite. Thus, Z_A is independent of scale, but depends on the lattice spacing a.

In this work, we shall adopt the third approach as mentioned above. It is known that Z_A as determined from the Ward identity has a small statistical error at the level of 0.2% [21] and will not contribute much to the overall error. When we study the quark mass dependence, we shall use the wave function renormalization from the quark propagator to obtain its dependence for the renormalization factors of the quark bilinear operators.

III. OVERLAP FERMION

The massless overlap-Dirac operator in lattice units is [14]

$$D(0) = [1 + \gamma_5\epsilon(H)], \tag{24}$$

where $\epsilon(H)$ is the matrix sign function of a Hermitian operator H. $\epsilon(H)$ depends on the background gauge field and has eigenvalues ± 1. Any such D is easily seen to satisfy the Ginsparg-Wilson relation [22]

$$\{\gamma_5, D\} = D\gamma_5 D. \tag{25}$$

For the topological sector with no zero modes, it follows easily that $\{\gamma_5, D^{-1}(0)\} = \gamma_5$ and by defining $\tilde{D}^{-1}(0) \equiv [D^{-1}(0) - 1/2]$ we see that it anticommutes with γ_5

$$\{\gamma_5, \tilde{D}^{-1}(0)\} = 0. \tag{26}$$

The standard choice of $\epsilon(H)(x, y)$ is $\epsilon(H) \equiv H_W/|H_W| = H_W/(H_W^\dagger H_W)^{1/2}$, where $H_W(x, y) = \gamma_5 D_W(x, y)$ is the Hermitian Wilson-Dirac operator. D_W is the usual Wilson-Dirac operator on the lattice. However, in the overlap formalism the Wilson mass parameter ρ needs to be negative in order to generate zero modes.

In the present work, we use the standard Wilson-Dirac operator, which can be written as

$$D_W(x,y) = \Big[\delta_{x,y} - \kappa \sum_{\mu} \{(r-\gamma_\mu) U_\mu(x) \delta_{y,x+\hat{\mu}} + (r+\gamma_\mu) U_\mu^\dagger(x-a\hat{\mu}) \delta_{y,x-\hat{\mu}}\} \Big]. \quad (27)$$

The negative Wilson mass $-\rho$ is then related to κ by

$$\kappa \equiv \frac{1}{2(-\rho)+8}. \quad (28)$$

ρ is chosen such that $\kappa > \kappa_c$ and $\rho < 2r$, and hence there is no species doubling and there can be zero modes for the massless quark. We take $r = 1$ and $\rho = 1.368$ (which corresponds to $\kappa = 0.19$) in our numerical simulation.

It is shown that the flavor nonsinglet scalar, pseudoscalar [23], vector, and axial [23,24] bilinears in the form $\bar{\psi} K T (1 - \frac{1}{2} D)\psi$ (K is the kernel which includes γ matrices and T is the flavor $SU(N_f)$ matrix) transform covariantly under the global chiral transformation $\delta\psi = T\gamma_5(1 - D/2)\psi$ as in the continuum. The $1 - \frac{1}{2}D$ factor is also understood as the lattice regulator which projects out the unphysical real eigenmodes of D at $\lambda = 2$. For the massive case, the fermion action is defined as $\bar{\psi}\rho D\psi + ma\bar{\psi}(1 - \frac{1}{2}D)\psi$ so that the tree-level wave function renormalization of the quark propagator is unity. In this case, the Dirac operator can be written as

$$D(m) = \rho D + ma\left(1 - \frac{1}{2}D\right) = \rho + \frac{m}{2} + \left(\rho - \frac{m}{2}\right)\gamma_5 \epsilon(H). \quad (29)$$

With the ψ field in the operators and the interpolation fields for hadrons replaced by the lattice regulated field $\hat{\psi} = (1 - \frac{1}{2}D)\psi$, the regulator factor will be associated with the quark propagator in the combination $(1 - \frac{1}{2}D)D(m)^{-1}$ in Green's functions, leading to an effective quark propagator [17]

$$S(x,y) = \left(1 - \frac{1}{2}D\right) D(m)^{-1} = (D_c + m)^{-1}, \quad (30)$$

where the operator $D_c = \rho D/(1 - \frac{1}{2}D)$ is chirally symmetric in the continuum sense, i.e. $\{\gamma_5, D_c\} = 0$ [25,26]; but, unlike D, it is nonlocal. Thus, the effective quark propagator in Eq. (30) turns out to have the same form as in the continuum, i.e. a chirally symmetric D_c plus a mass term in the inverse propagator [17,27–29]. By studying the dispersion relation of the pseudoscalar and vector mesons, it is learned [17] that the $(ma)^2$ errors are much smaller than those of the Wilson fermion, making it a viable option for studying the heavy-light systems. Furthermore, it affords a nonperturbative renormalization of the heavy-light decay constant via the chiral Ward identity and the unequal mass Gell-Mann-Oakes-Renner relation [17]. The preliminary study of the charmonium spectrum with the quenched overlap fermion seems encouraging as far as the hyperfine splitting and the S-wave to P-wave charmonium splittings are concerned [30].

IV. NUMERICAL RESULTS

In this paper we work on a $16^3 \times 28$ lattice with lattice spacing, $a = 0.20$ fm, as determined from the pion decay constant f_π [31]. The gauge configurations are created by the Iwasaki gauge action through the pseudoheat-bath algorithm. A total of 80 configurations are used. The lattice parameters are summarized in Table I.

Recently it has been speculated [32] that the overlap operator with coarse lattice spacing of 0.2 fm, such as in Ref. [31] and this study, might have a range as large as 4 lattice units. Thus, the calculations might be afflicted by unphysical degrees of freedom as light as 0.25 GeV. It has been shown [33] by direct calculations at lattice spacings of 0.2 fm, 0.17 fm, and 0.13 fm that this is not the case. The range of the overlap operator as defined in Ref. [34] is about 1 lattice unit (in Euclidean distance or 2 units of "taxi driver" distance) for each of the above lattice spacings. Therefore, the range of the overlap-Dirac operator scales to zero in physical units in the continuum limit and our $16^3 \times 28$ lattice, with spacing of 0.2 fm, used in this study is in the scaling range.

The gauge field configurations are gauge fixed to the Landau gauge using a conjugate gradient fourier acceleration [35] algorithm with an accuracy of $\theta \equiv \sum |\partial_\mu A_\mu(x)|^2 < 10^{-12}$. We use an improved gauge-fixing scheme [36] to minimize gauge-fixing discretization errors. Since gauge fixing is involved for the external quark state, there are concerns about the effects of Gribov copies on the numerical results of the renormalization procedure. A study of two different realization of the Landau gauge and a covariant gauge shows that the renormalization constants from these gauge fixings differ by less than the statistical errors of about 1%–1.5% level [37]. We shall thus assume that the potential uncertainty due to Gribov copies is at this 1%–1.5% level which is comparable to our statistical errors.

Our numerical calculation begins with an evaluation of the inverse of $D(m)$ which is defined in Eq. (29). We use a 14th-order Zolotarev approximation [38] to the matrix sign function $\epsilon(H_W)$. In the selected window of $x \in [0.031, 2.5]$ of $\epsilon(x)$, the approximation is better than 3.3×10^{-10} [31].

TABLE I. Lattice parameters.

Action	Volume	N_{Therm}	N_{Samp}	β	a (fm)	Physical Volume (fm^4)
Iwasaki	$16^3 \times 28$	10000	5000	2.264	0.200	$3.2^3 \times 5.60$

We then calculate Eq. (30) for each configuration by using multimass conjugate gradient method for both the inner and outer loops. The detailed numerical description is given in Ref. [31]. In the calculations, $\kappa = 0.19$ was used, which corresponds to $\rho = 1.368$. We calculate 15 quark masses by using a shifted version of the conjugate gradient solver [16,19]. The bare quark masses ma are chosen to be $ma = 0.021\,00$, $0.030\,33$, $0.044\,33$, $0.064\,17$, $0.075\,83$, $0.089\,83$, $0.108\,50$, $0.129\,50$, $0.156\,33$, $0.187\,83$, $0.226\,33$, $0.268\,33$, $0.322\,00$, $0.400\,00$, and $0.600\,00$. With the scale determined by f_π, they correspond to pion masses 212(7), 247(6), 290(6), 342(6), 370(7), 400(7), 438(7), 478(8), 524(8), 575(9), 633(10), 692(11), 764(12), 862(13), 1092(17) MeV, respectively [31].

In the following, we give the steps for the numerical calculation:

(a) After we calculate the quark propagators in coordinate space for each configuration, we use the Landau gauge transformation matrix to rotate the quark propagators to the Landau gauge. The discrete Fourier transform is then used to calculate the quark propagators in momentum space.

(b) Next, we calculate the five projected vertex functions $\Gamma_O(pa)$ defined in Eq. (12), where we have used the effective quark propagator in Eq. (30) for the calculation. By definition, they are the ratios of renormalization constants at the chiral limit (i.e. $Z_\psi(\mu a, g(a))/Z_O(\mu a, g(a))$ from Eq. (14)) in the RI scheme at scale $\mu^2 = p^2$. They are in general dependent on $(pa)^2$ which comes from two sources. One is from the running of the renormalization constants in the RI scheme; the other is from the possible $(pa)^2$ error.

(c) We decouple the two above mentioned scale dependencies of the calculated $\Gamma_O(pa)$ by first dividing out its perturbative running in the RI scheme. Ideally, this should take care of the scale dependence, since we have taken the scale to infinity. However, due to the $(pa)^2$ error on the lattice, there can still be some $(pa)^2$ dependence in the $\Gamma_O(pa)$ after undoing the perturbative running. Following Ref. [9], we shall attribute the remaining scale dependence to the $(pa)^2$ error and will use the simple linear fit to remove it. This will be discussed in Section V. For the scalar and pseudoscalar vertex functions, there is an additional complication due to the presence of quark mass poles [9]. We shall remove them first and then extrapolate to the chiral limit. Finally, we can check the expected relations $Z_A = Z_V$ and $Z_S = Z_P$.

(d) In order to compare results with experiments, one frequently quotes the scale-dependent results in the $\overline{\text{MS}}$ scheme at certain scale. So the final step is to perturbatively match the results from the RI scheme to the $\overline{\text{MS}}$ scheme at $\mu = 2$ GeV for Z_S, Z_P, Z_T, and Z_ψ.

A. Axial and vector currents

Let us consider first the vector and axial-vector currents. Since each obeys a Ward Identity [39], their renormalization constants are finite. In Fig. 1, we show the vertex functions Γ_A and Γ_V from Eq. (12) for different bare quark masses as a function of the lattice momentum $(pa)^2$. We find that they are weakly dependent on the mass, and almost scale independent after $(pa)^2 \geq 2.0$, which corresponds to $p \geq 1.4$ GeV.

In the RI scheme, Eq. (14) implies that in the chiral limit

$$\lim_{m\to 0}\Gamma_{A/V}(pa)|_{p^2=\mu^2} = Z_\psi(\mu a, g(a))/Z_{A/V}, \qquad (31)$$

and one expects that $Z_A = Z_V$ for the overlap fermion, but this is true only for large momenta p. At low momenta, Γ_A and Γ_V may differ due to the effects of spontaneous chiral-symmetry breaking [9].

Following Ref. [9], we show in Fig. 2 the quantities $\Gamma_A - \Gamma_V$ and $\frac{1}{2}(\Gamma_A + \Gamma_V)$, after linearly extrapolating with respect to ma to the chiral limit. We can observe from the upper panel of the figure that there is no effect

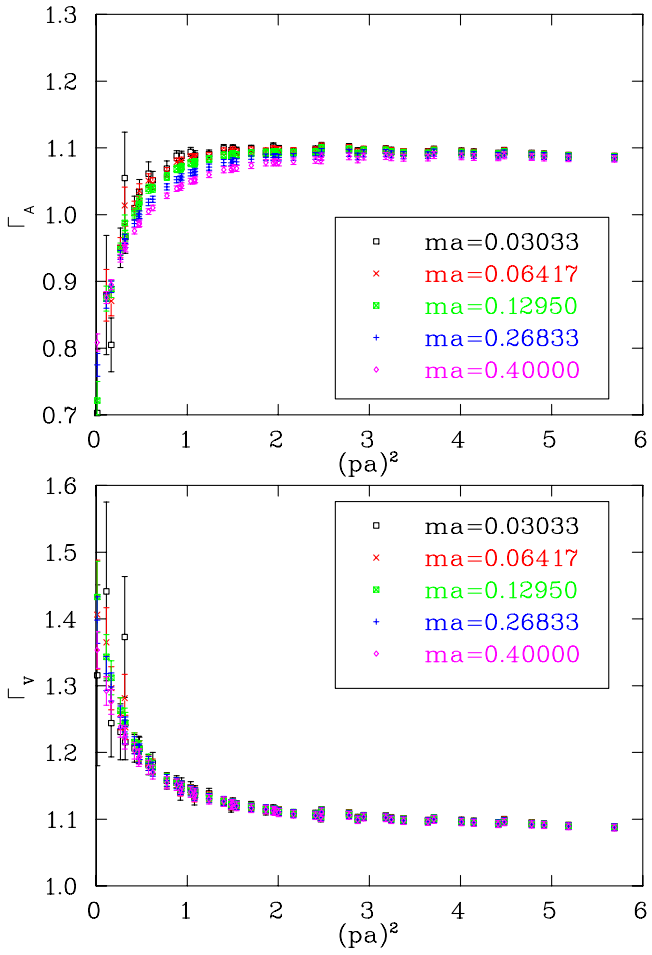

FIG. 1 (color online). The projected vertex function Γ defined in Eq. (12) for the vector and axial-vector currents with different bare quark masses.

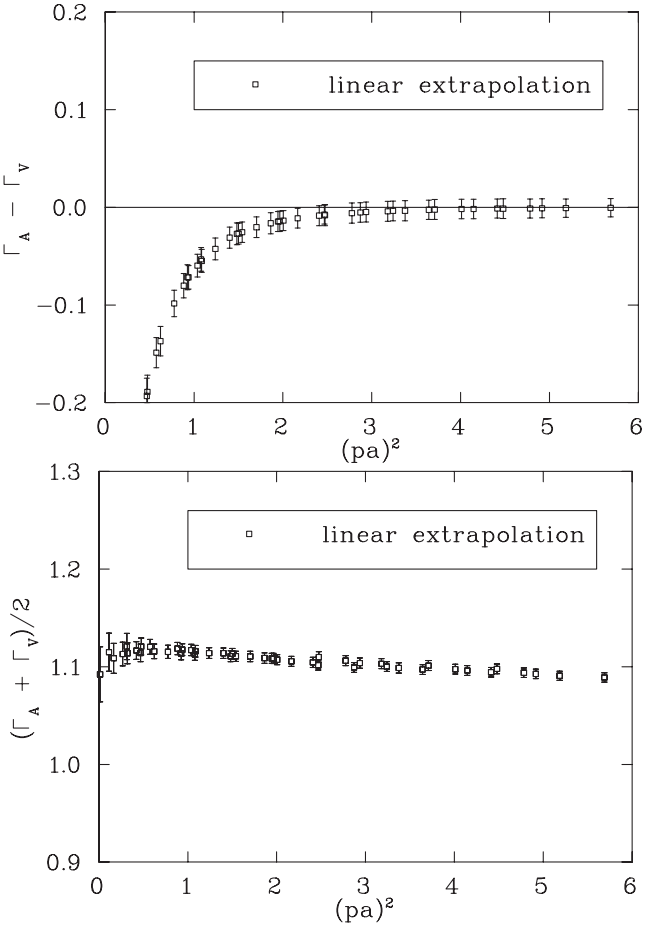

FIG. 2. The upper panel is $(\Gamma_A - \Gamma_V)$ versus $(pa)^2$. We see that $Z_A = Z_V$ is valid above moderate $(pa)^2 \sim 2.5$. Here we linear extrapolate to the chiral limit ($m = 0$) with respect to ma. The lower panel is $\frac{1}{2}(\Gamma_A + \Gamma_V)$ versus $(pa)^2$.

of spontaneous chiral-symmetry breaking at moderate and high momenta, where $\Gamma_A - \Gamma_V$ tends to zero. In fact, the percentage error between Γ_A and Γ_V is less than 1% at $(ap)^2 = 2.5$ (top panel) and is comparable to the statistical error. This deviation decreases further for higher momenta. On the other hand, the effects of spontaneous chiral-symmetry breaking are clearly visible at low momenta where Γ_A and Γ_V differ. In the lower panel of Fig. 2, we plot $\frac{1}{2}(\Gamma_A + \Gamma_V)$ against $(pa)^2$. Since Z_V and Z_A are scale independent, the slight $(pa)^2$ dependence that one observes in $\frac{1}{2}(\Gamma_A + \Gamma_V)$ in Fig. 2 for $(pa)^2 > 2.5$ reflects the scale dependence of Z_ψ and the lattice $(pa)^2$ error.

B. Pseudoscalar and scalar densities

The pseudoscalar and scalar densities differ from the axial and vector currents in the sense that their renormalization constants are not scale independent. The scalar and pseudoscalar densities with the form $\bar{\psi}(1 - D/2)\psi$ and $\bar{\psi}\gamma_5(1 - D/2)\psi$ transform under the lattice chiral transformation as in the continuum [15,40,41]. From the Ward identities, one obtains the relations

$$Z_S = Z_P, \tag{32}$$

$$Z_m = \frac{1}{Z_S}. \tag{33}$$

Thus, the quantities Z_S/Z_P, $Z_S Z_m$, and $Z_m Z_P$ are expected to be scale independent.

For the case of the pseudoscalar and scalar renormalization, there is a complication due to the presence of the quark condensate in the inverse quark propagator. Using the axial Ward identity from the quark propagator, one has [9]

$$m\Gamma_P(p, p) = \tfrac{1}{12}\mathrm{Tr}(S^{-1}(p)). \tag{34}$$

It is known that due to the spontaneous chiral-symmetry breaking, the trace of the inverse quark propagator picks up a contribution from the quark condensate [42]. At large p^2 [42], it is given by

$$\frac{1}{12}\mathrm{Tr}(S^{-1}(p)) = m - \langle\bar{q}q\rangle\frac{4\pi\alpha_s}{3p^2} + O(1/p^4) \tag{35}$$

from first order perturbation [42]. This implies that the renormalized $\mathrm{Tr}(S^{-1}_{\mathrm{ren}}(p))$ should be

$$\frac{1}{12}\mathrm{Tr}(S^{-1}_{\mathrm{ren}}(p)) = m_{\mathrm{ren}} - C_1\frac{\langle\bar{q}q\rangle}{p^2} + O(1/p^4). \tag{36}$$

In the study of lattice artifacts of the Wilson fermion [43], it is shown that there are three terms which mix at $O(a)$ to give an improved and renormalized quark field,

$$q_{\mathrm{ren}} = Z_\psi^{1/2}(1 + b_q ma)\{1 + ac'_q(\not{p} + m_{\mathrm{ren}}) + ac_{NGI}\not{\partial}\}q_0, \tag{37}$$

where $\not{\partial}$ may appear due to gauge fixing. It is found [43] in the study of the order $O(a)$ error of Wilson fermion, that c'_q is large. Combining Eqs. (36) and (37), one has [9]

$$\begin{aligned}\frac{1}{12}\mathrm{Tr}(S^{-1}_{\mathrm{latt}}(pa)) = \ldots &+ Z_m Z_\psi(ma + m_{\mathrm{res}}a) \\ &- C_1 Z_\psi\frac{a^3\langle\bar{q}q\rangle}{(pa)^2} + 2(c_{NGI} - c'_q)(pa)^2 \\ &+ O(1/p^4),\end{aligned} \tag{38}$$

where terms of $O(mc_{NGI})$ are neglected. Thus, in this case, $\frac{1}{12}\mathrm{Tr}(S^{-1}_{\mathrm{latt}}(pa))$ diverges for large pa.

On the other hand, it is learned from the domain-wall fermion [9] study on a $16^3 \times 32 \times 16$ lattice with Wilson gauge action at $\beta = 6.0$, the explicit chiral-symmetry breaking effect from the $c_{NGI} - c'_q$ term is negligible for moderately large values of $(pa)^2$ and that the residual mass is small. Since the explicit symmetry breaking is controlled to a level $<10^{-9}$ with the Zoloterav approximation of the sign function [31] for the overlap fermion, we expect the $c_{NGI} - c'_q$ term to be negligibly small. It was already

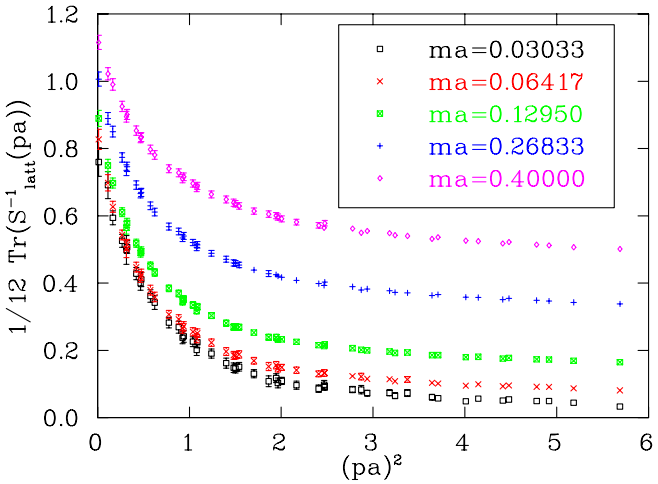

FIG. 3 (color online). A plot of $\frac{1}{12}\mathrm{Tr}(S^{-1}_{\mathrm{latt}}(pa))$ versus $(pa)^2$ for different bare quark mass ma on $16^3 \times 28$ lattice, showing that $\frac{1}{12}\mathrm{Tr}(S^{-1}_{\mathrm{latt}}(pa))$ approaches a constant value at large $(pa)^2$.

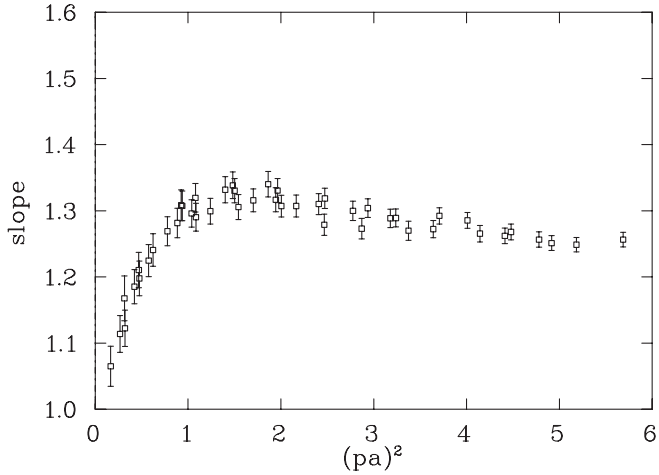

FIG. 5. A plot of the slope of $\frac{1}{12}\mathrm{Tr}(S^{-1}_{\mathrm{latt}}(pa))$ with respect to the quark mass as a function of $(pa)^2$. It is expected to be $Z_m Z_\psi$ at large $(pa)^2$ from Eq. (38).

shown that the residual quark mass due to the numerical approximation of the overlap operator is negligible [19]. Here, we shall verify the expectation that the $c_{NGI} - c'_q$ term is indeed negligible.

As shown in Fig. 3, $\frac{1}{12}\mathrm{Tr}(S^{-1}_{\mathrm{latt}}(pa))$ for several quark masses tend to constant values after $(pa)^2 \geq 4$. This indicates that there is no discernible contamination due to the explicit chiral-symmetry term $2(c_{NGI} - c'_q)(pa)^2$ which grows as $(pa)^2$. Figure 4 shows the same at the chiral limit which is obtained from linear extrapolation in ma. In this case, $\frac{1}{12}\mathrm{Tr}(S^{-1}_{\mathrm{latt}}(pa))$ tends to zero at large $(pa)^2$ as expected from Eq. (38) with no residual mass. Plotted in Fig. 5 is the slope of $\frac{1}{12}\mathrm{Tr}(S^{-1}_{\mathrm{latt}}(pa))$ with respect to the quark mass ma. It is expected to be $Z_m Z_\psi$ at large $(pa)^2$ from Eq. (38). These results are very similar to those of the domain-wall fermion [9].

From Eqs. (34) and (38), one finds that

$$\Gamma_P(pa, pa) = \frac{Z_\psi}{Z_P} - C_1 Z_\psi \frac{a^3\langle\bar{q}q\rangle}{ma(pa)^2} + O(1/p^4). \quad (39)$$

Since the quark condensate $\langle\bar{q}q\rangle$ has a contribution of $\frac{\langle|Q|\rangle}{mV}$ from the zero modes due to the topological charge Q, it is expected that $\Gamma_P(pa, pa)$ has $1/m^2$ and $1/m$ singularities as $m \to 0$. Thus, it is suggested [9] to fit $\Gamma_P(pa, pa)$ with the functional form involving pole terms. As illustrated in Fig. 6, the singular behavior in m is quite visible. It is suggested in Ref. [9] to fit the Γ_P with a double and single pole form for each pa

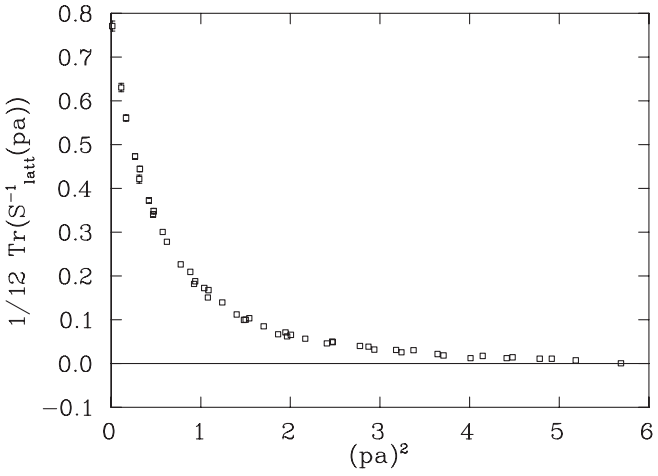

FIG. 4. The value of $\frac{1}{12}\mathrm{Tr}(S^{-1}_{\mathrm{latt}}(pa))$ extrapolated to $m = 0$ vs $(pa)^2$ by a simple linear extrapolation. At large $(pa)^2$, the extrapolated value is zero within errors.

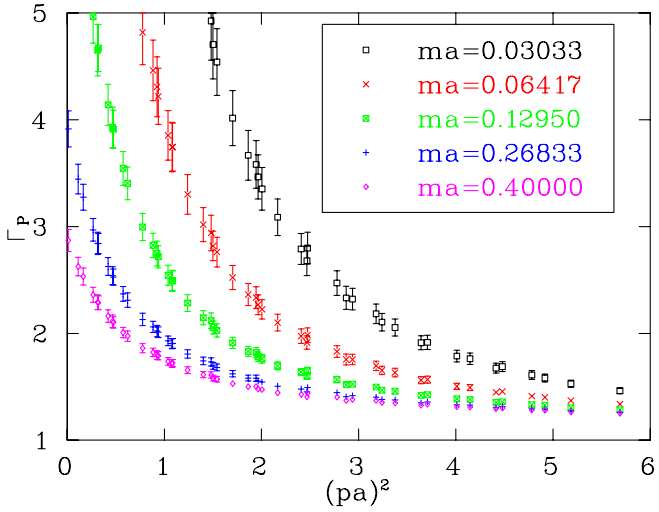

FIG. 6 (color online). Γ_P versus $(pa)^2$ with different masses. Here, one can clearly see the strong divergent behavior for small quark masses.

$$\Gamma_P(pa, pa) = \frac{c_{1,P}}{(am)^2} + \frac{c_{2,P}}{(am)} + c_{3,P} + c_{4,P}(am)^2. \quad (40)$$

This is appropriate for the case studied in Ref. [9] where the lattice volume is relatively small (the space-time volume is ~ 10 fm^4) so that the zero mode contribution is substantial and the quark mass is relatively heavy so that the quenched chiral log is not significant. In our case, the space-time volume at 184 fm^4 is much larger. As such, the zero mode contribution is expected to be smaller. In our study of the quenched chiral log in the pion mass [31] with the same lattice, it is found that the pion mass is basically the same when calculated from either the $\langle PP\rangle$, $\langle A_4P\rangle$, $\langle A_4A_4\rangle$, or $\langle PP - SS\rangle$ correlators, indicating that the zero mode effects are small and negligible within statistical errors, even for the smallest pion mass at ~ 180 MeV. Our lowest pion mass is 212 MeV in the current study. On the other hand, the quenched chiral log is quite prominent with pion mass less than 400 MeV. Therefore, we believe that the more appropriate approach is to relate the quark condensate in Eq. (39) to the pion mass through the Gell-Mann-Oakes-Renner relation

$$\langle \bar{q}q\rangle = -\frac{m_\pi^2 f_\pi^2}{2m}, \quad (41)$$

and use the power form for the pion mass where the leading log is resummed through the cactus diagrams [44], i.e.

$$m_\pi^2(ma) = A(ma)^{1/(1+\delta)} + B(ma)^2. \quad (42)$$

Here δ is the quenched chiral log parameter.

Neglecting higher order terms and expanding $f_\pi \simeq f_\pi(0) + c(ma)$, we can approximate Eq. (39) as

$$\Gamma_{P,\mathrm{latt}}(ap, ma) \simeq A_1\{(ma)^{[1/(1+\delta)]-2} + a_P(ma)^{[1/(1+\delta)]-1}\} + A_2 + C_P(ma^2) + D_P(ma)^2, \quad (43)$$

where

$$A_1 = \frac{Aa^3 f_\pi^2(0)}{2(pa)^2} C_1 Z_\psi, \qquad a_P = \frac{c}{f_\pi(0)}, \qquad A_2 = \frac{Ba^3 f_\pi^2(0)}{2(pa)^2} C_1 Z_\psi + Z_m Z_\psi. \quad (44)$$

We plot $\Gamma_P(pa, pa)$ in Fig. 6 as a function of $(pa)^2$ for several ma. It is clear that at small $(pa)^2$, it has a singular behavior for small ma which is presumably due to the divergent terms associated with the quenched chiral δ.

For Γ_S, it also displays a singular behavior as shown in Fig. 7. From the vector Ward identity, one has the relation

$$\Gamma_S = \frac{1}{12}\frac{\partial \mathrm{Tr}[S(p)^{-1}]}{\partial m}. \quad (45)$$

From Eq. (38), the above Γ_S can be approximated with

$$\Gamma_S(pa, pa) = \frac{Z_\psi}{Z_S} + \frac{C_1 Z_\psi}{(pa)^2}\frac{\partial a^3\langle \bar{q}q\rangle}{\partial ma} + \ldots \quad (46)$$

for large $(pa)^2$.

Similar to the pseudoscalar case, substituting the pion mass in Eq. (42) and the Gell-Mann-Oakes-Renner relation in Eq. (41) to Eq. (45) and neglecting the higher order terms beyond $(ma)^2$, we obtain

$$\Gamma_{S,\mathrm{latt}}(ap, ma) = A_1\left\{-\frac{\delta}{1+\delta}(ma)^{[1/(1+\delta)]-2} + a_S\frac{1}{1+\delta}(ma)^{[1/(1+\delta)]-1}\right\} + A_2 + C_S(ma^2) + D_S(ma)^2. \quad (47)$$

At first glance, it appears that the quantity $Z_m Z_\psi$ in A_2 is not separable from the other term in Eq. (44). However, we should note that we know the values of A, B, and $f_\pi(0)$ in Eq. (44) from an earlier study of the pion mass and decay constant [31]. After fitting A_1 and A_2 in Eqs. (43) and (47), one can compare the first term in A_2 with A_1 to obtain $Z_m Z_\psi$. As we shall see later, it turns out the first term in A_2 is $O(10^{-2})$ times smaller than $Z_m Z_\psi$.

In order to obtain $Z_m Z_\psi$ and assess its finite m behavior, we first subtract the divergent terms in Eqs. (43) and (47) and then fit the subtracted vertex functions linear and quadratic in m, i.e. with ma^2 and m^2a^2 terms. In the following subsection, we shall detail our fitting methods and give the results. We should note in passing that it has been suggested to use nondegenerate quark masses to avoid the divergence in Γ_P [11,45]. However, due to the complication of the quenched chiral log, it is not applicable here.

1. Fitting

We adopt the fitting procedure used to fit the chiral logs in the pion mass [31] and the Roper resonance in the nucleon correlator [46] with priors. From the chiral log fit of the pion mass [31], we obtain δ to be in the range of 0.20–0.15 when the maximum pion mass for the fitting

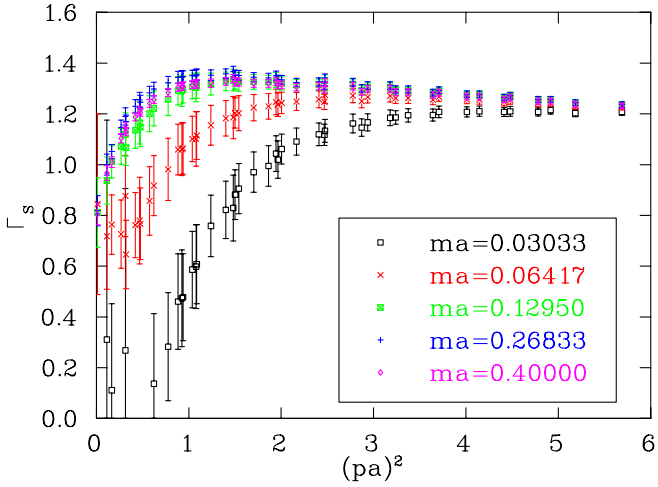

FIG. 7 (color online). Γ_S versus $(pa)^2$ with different masses. The chiral log behavior is also quite visible.

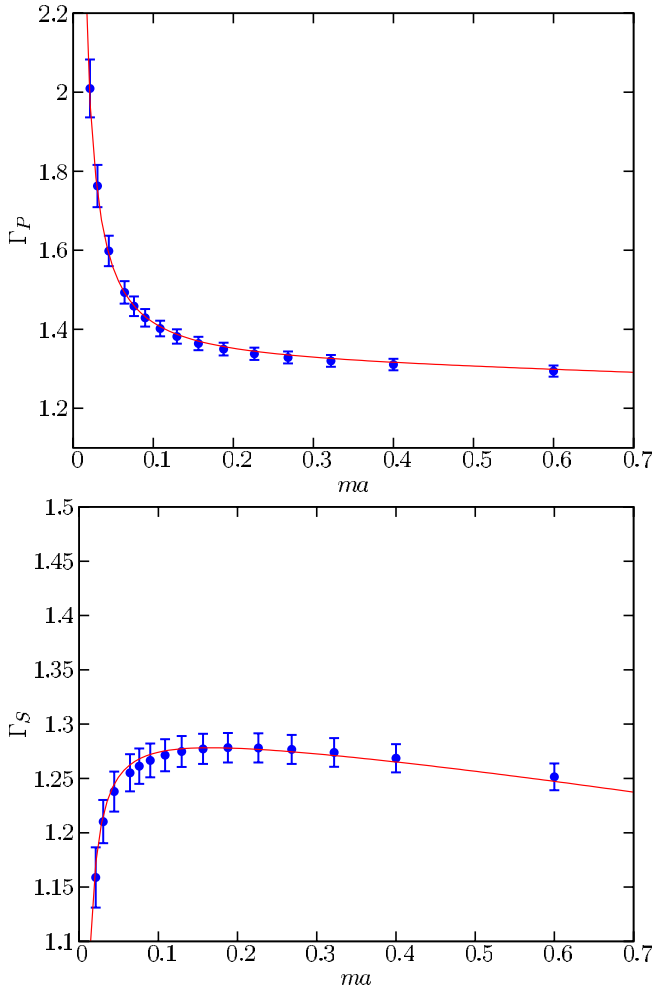

FIG. 8 (color online). Vertex functions for scalar (top) and pseudoscalar (bottom) channels at the momentum corresponding to $\mu = 2$ GeV.

range is set to be ~500-900 MeV. Since we are fitting Γ_P and Γ_S in the similar quark mass range, we put a weak constraint on the value of δ with $\delta = 0.18(5)$ which covers the range of δ in the fit of the quenched chiral log in the pion mass. Data corresponding to the few lowest masses are first fitted with $A_{1P}(A_{1S})$, $a_P(a_S)$, and $A_{2P}(A_{2S})$ and then these parameters are constrained with those fitted values to fit the whole range of the masses with the forms in Eqs. (43) and (47). It is observed that these vertex functions are highly correlated between different masses and that the correlation increases with higher momentum. This, we believe, is due to the fact that the quark masses that we are interested in are all much smaller than the external momentum of $pa = 4.145$ which corresponds to $\mu = 2$ GeV that we will use to eventually match to the $\overline{\text{MS}}$ scheme at this scale. In this sense, the high correlation is a generic feature that this nonperturbative renormalization procedure faces for light quarks.

We show in Fig. 8 the vertex functions $\Gamma_P(pa, ma)$ and $\Gamma_S(pa, ma)$ at $pa = 4.145$ as a function of ma, together with the fitted curves based on Eqs. (43) and (47). The fitted parameters are given in Table II. We see from the fitted parameters A_1, $a_P(a_S)$, δ, and A_2 from Γ_P agree with those fitted from Γ_S, respectively, as we expected. This supports our supposition that the singular behaviors in both the $\Gamma_P(pa, ma)$ and $\Gamma_S(pa, ma)$ are due to the quenched chiral log in $\langle\bar{q}q\rangle$. We also tried to fit the pseudoscalar vertex function in the form in Eq. (40) and found that it does not fit well—the χ^2 is too large.

We note that the fitted central values of δ tend to be on the low side compared to our previous fit of the pion mass which gives $\delta = 0.20(3)$ [31] and is in agreement with $\delta \sim 0.23$ as deduced from the topological susceptibility calculation with the overlap operator [47]. We think the reason is that the smallest quark mass in the present fit which corresponds to $m_\pi \sim 250$ MeV is larger than that in the previous fitting of the pion mass which corresponds to $m_\pi \sim 180$ MeV. According to the detailed study [31] of the quenched chiral log as a function of the fitting range of quark masses, this behavior of a smaller δ for a higher quark mass range is to be expected.

When we take the value of $A = 1.3$ and $B = 1.1$ from our pion mass chiral log fit (Fig. 12 in Ref. [31]) in the relevant mass range, it follows from Eq. (44) that

$$R = \frac{Ba^3 f_\pi^2(0)}{2(pa)^2} C_1 Z_\psi = \frac{BA_1}{A} = 0.0068, \qquad (48)$$

which is 2 orders of magnitude smaller than A_2. We shall subtract this contribution from A_2 in Eq. (44) to obtain $Z_m Z_\psi$ which changes its value by about half a σ which is not significant.

To eventually obtain Z_S and Z_P and their respective finite m dependence, we define the subtracted Γ_P and Γ_S by taking out the divergent terms in Eqs. (43) and (47) and the first term in A_2 in Eq. (44) on each Jackknife sample (J) as

TABLE II. Fitted parameters corresponding to Eqs. (43) and (47).

Channel	A_1	$a_P(a_S)$	δ	A_2	C	D	χ^2/dof
P	0.008(1)	0.08(9)	0.163(18)	1.305(15)	−0.024(6)	−0.022(5)	1.29
S	0.011(5)	0.14(42)	0.171(24)	1.302(17)	−0.079(8)	−0.020(5)	1.47

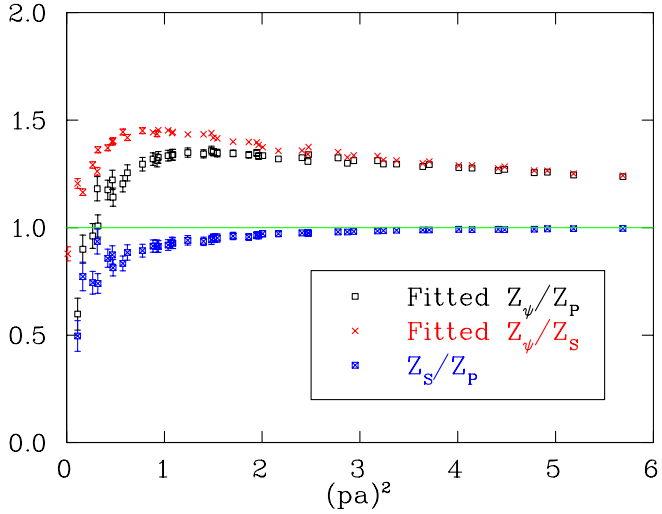

FIG. 9 (color online). Z_ψ/Z_P and Z_ψ/Z_S and the ratio Z_P/Z_S as a function of $(pa)^2$.

$$\Gamma_P^{\mathrm{sub},J}(ma) = \Gamma_P^J(ma) - A_{1J}^P\{(ma)^{[1/(1+\delta_J)]-2} + a_J^P(ma)^{[1/(1+\delta_J)]-1}\} - \frac{BA_{1J}^P}{A}, \quad (49)$$

$$\Gamma_S^{\mathrm{sub},J}(ma) = \Gamma_S^J(ma) - A_{1J}^S\left\{-\frac{\delta_J}{1+\delta_J}(ma)^{[1/(1+\delta_J)]-2} + \frac{a_J^S}{1+\delta_J}(ma)^{[1/(1+\delta_J)]-1}\right\} - \frac{BA_{1J}^S}{A}. \quad (50)$$

From Eqs. (43), (44), (47), and (49), we see that the ratios of Z_ψ/Z_P and Z_ψ/Z_S are the subtracted vertices Γ_P and Γ_S at the massless limit for each pa in the RI scheme, i.e.

$$\frac{Z_\psi(pa)}{Z_{P,S}(pa)} = \Gamma_{P,S}^{sub}(pa, ma = 0). \quad (51)$$

We plot in Fig. 9, Z_ψ/Z_P, Z_ψ/Z_S, and the ratio Z_S/Z_P as a function of $(pa)^2$. We see that for $(pa)^2 > 3$, the ratio goes to unity which is a confirmation that our fitting procedure does not spoil the expected chiral property $Z_P = Z_S$ for the overlap fermion.

C. The tensor current

In Fig. 10, we show Γ_T versus $(pa)^2$ with different masses. We can see that at moderate to large $(pa)^2$, Γ_T is not sensitive to the quark masses. The chiral limit value is obtained by a linear plus quadratic fitting as for the case of vector and axial-vector currents and the results will be presented in the next section.

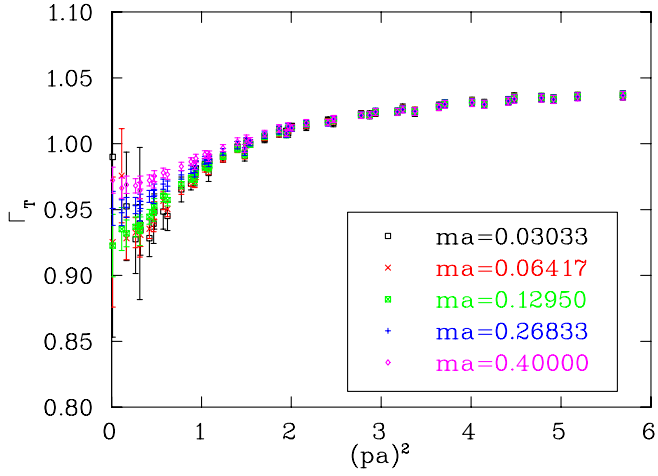

FIG. 10 (color online). Γ_T versus $(pa)^2$ with different masses. It has no significant mass dependence.

V. RUNNING OF THE RENORMALIZATION CONSTANTS

In general, one can choose to define the renormalization conditions for different p and p' in Eq. (10). But the virtuality of the quark states must be much larger than Λ_{QCD}. This is so because in order to obtain physical results at certain scale (e.g. momentum or mass), one needs to combine the matrix element of the renormalized operator $O(\mu)$ with the Wilson coefficient function. The latter is usually computed in continuum perturbation theory by expanding in $\alpha_s^{\overline{\mathrm{MS}}}$ at a scale of order of μ. Thus, for the validity of perturbation calculation, μ must be large. On the other hand, one would like to have $\mu \ll 1/a$ in order to have smaller $O(a)$ effects. When spontaneous symmetry breaking takes place, as is in QCD, a large μ may not be enough due to the presence of the Goldstone boson. For example, at low momentum transfer $q = p' - p$, the Green's function can have a Goldstone boson pole like $1/q^2$. However for fermions (but not for a scalar particle), this contribution will be $1/p^2 = 1/\mu^2$ smaller than the perturbative contribution even when $q^2 = 0$ [1]. Thus, it is desirable to have a window $\Lambda_{\mathrm{QCD}} \ll \mu \ll 1/a$ so that both the nonperturbative effects and the lattice artifacts are small. In practice, one finds that the renormalization procedure prescribed here works well for $(\mu a)^2$ as large as 6. In the current case, this corresponds to $\mu \sim 2.5$ GeV.

The renormalized operators are defined as

$$Z_O O_{\mathrm{bare}} = O_{\mathrm{ren}}. \quad (52)$$

The fact that the bare operator is independent of the renormalization scale μ^2 gives the renormalization group (RG) equation,

$$\mu^2 \frac{d}{d\mu^2} O_{\mathrm{ren}} = \frac{1}{Z_O}\mu^2 \frac{dZ_O}{d\mu^2} O_{\mathrm{ren}} \quad (53)$$

$$= -\frac{\gamma_O}{2} O_{\rm ren}, \tag{54}$$

where

$$\gamma_O = -\frac{2\mu^2}{Z_O}\frac{dZ_O}{d\mu^2}, \tag{55}$$

is the anomalous dimension.

The solution of $Z_O(\mu^2)$ can be written in the following form

$$Z_O(\mu^2) = \frac{C_O(\mu^2)}{C_O(\mu'^2)} Z_O(\mu'^2). \tag{56}$$

Expanding the anomalous dimension in the coupling constant α_s

$$\gamma_O = \sum_i \gamma_O^{(i)} \left(\frac{\alpha_s}{4\pi}\right)^{i+1}, \tag{57}$$

and considering the running of α_s in QCD β function $\beta(\alpha_s)$ perturbatively

$$\frac{\beta(\alpha_s)}{4\pi} = \mu^2 \frac{d}{d\mu^2}\left(\frac{\alpha_s}{4\pi}\right) = -\sum_{i=0}^{\infty} \beta_i \left(\frac{\alpha_s}{4\pi}\right)^{i+2}, \tag{58}$$

where β_i are the coefficients of the QCD β function $\beta(\alpha_s)$, one can solve for the coefficient functions C_O perturbatively.

The four loop solution [48] of the coefficient function in Eq. (56) is (we have suppressed the subscripts for the specific operator O)

$$\begin{aligned} C(\mu^2) = \left(\frac{\alpha_s(\mu)}{\pi}\right)^{\bar\gamma_0} \Bigg\{ & 1 + \left(\frac{\alpha_s(\mu)}{4\pi}\right)(\bar\gamma_1 - \bar\beta_1\,\bar\gamma_0) + \frac{1}{2}\left(\frac{\alpha_s(\mu)}{4\pi}\right)^2 [(\bar\gamma_1 - \bar\beta_1\,\bar\gamma_0)^2 + \bar\gamma_2 + \bar\beta_1{}^2\bar\gamma_0 - \bar\beta_1\,\bar\gamma_1 - \bar\beta_2\,\bar\gamma_0] \\ & + \left(\frac{\alpha_s(\mu)}{4\pi}\right)^3 \Bigg[\frac{1}{6}(\bar\gamma_1 - \bar\beta_1\,\bar\gamma_0)^3 + \frac{1}{2}(\bar\gamma_1 - \bar\beta_1\,\bar\gamma_0)(\bar\gamma_2 + \bar\beta_1{}^2\bar\gamma_0 - \bar\beta_1\,\bar\gamma_1 - \bar\beta_2\,\bar\gamma_0) \\ & + \frac{1}{3}(\bar\gamma_3 - \bar\beta_1{}^3\bar\gamma_0 + 2\bar\beta_1\,\bar\beta_2\,\bar\gamma_0 - \bar\beta_3\,\bar\gamma_0 + \bar\beta_1{}^2\bar\gamma_1 - \bar\beta_2\,\bar\gamma_1 - \bar\beta_1\,\bar\gamma_2) \Bigg] \Bigg\}, \end{aligned} \tag{59}$$

where

$$\bar\gamma_i = \frac{\gamma^{(i)}}{2\beta_0}, \qquad \bar\beta_i = \frac{\beta_i}{\beta_0}. \tag{60}$$

Tables III, IV, and V give the anomalous dimensions $\gamma^{(i)}$ for Z_ψ, Z_m, and Z_T in the RI/MOM scheme for the quenched approximation [20,48,49]. In the case of chiral fermions, $Z_S = Z_P = 1/Z_m$, so that $C_S(\mu^2) = C_P(\mu^2) = 1/C_m(\mu^2)$. Note that, in Refs. [20,48,49], the definition of Z's is the inverse of our definition in Eq. (52).

The coupling constant itself is running with respect to μ. The four loop formula is given by [50]

$$\begin{aligned} \frac{\alpha_s}{4\pi} = & \frac{1}{\beta_0 \ln(\mu^2/\Lambda^2_{\rm QCD})} - \frac{\beta_1 \ln\ln(\mu^2/\Lambda^2_{\rm QCD})}{\beta_0^3 \ln^2(\mu^2/\Lambda^2_{\rm QCD})} + \frac{1}{\beta_0^5 \ln^3(\mu^2/\Lambda^2_{\rm QCD})} \{\beta_1^2 \ln^2 \ln(\mu^2/\Lambda^2_{\rm QCD}) - \beta_1^2 \ln\ln(\mu^2/\Lambda^2_{\rm QCD}) + \beta_2\beta_0 - \beta_1^2\} \\ & + \frac{1}{\beta_0^7 \ln^4(\mu^2/\Lambda^2_{\rm QCD})} \Big\{ \beta_1^3 \ln^3 \ln(\mu^2/\Lambda^2_{\rm QCD}) - \frac{5}{2}\beta_1^3 \ln^2 \ln(\mu^2/\Lambda^2_{\rm QCD}) - (2\beta_1^3 - 3\beta_0\beta_1\beta_2) \ln\ln(\mu^2/\Lambda^2_{\rm QCD}) \\ & + \frac{1}{2}(\beta_1^3 - 3\beta_0^2\beta_3) \Big\}. \end{aligned} \tag{61}$$

The QCD β function is scheme independent only up to two loops. The additional terms of the expansion have been computed in the $\overline{\rm MS}$ scheme in Ref. [51].

In this work, the value of α_s was calculated at four loops using a lattice value of $\Lambda_{\rm QCD}$ taken from Ref. [52] as

$$\Lambda_{\rm QCD} = 238 \pm 19 \text{ MeV}. \tag{62}$$

Both Z_A and Z_V are scale independent, but this is not the case for Z_ψ. The scale invariant (SI) vertex for the axial and vector current is defined by removing the renormalization group running of Z_ψ as

$$\Gamma^{\rm SI}_{A,V}((ap)^2) = \Gamma_{A,V}((ap)^2)/C_\psi((ap)^2), \tag{63}$$

where C_ψ is defined in Eq. (59) with the anomalous dimension coefficients from Table III. We normalize $C_\psi((\mu a)^2 = 4.15) = 1$, which corresponds to $\mu = 2.0$ GeV, in order to compare with the $(pa)^2$ dependence of $\Gamma_{A,V}((ap)^2)$.

TABLE III. Quenched Z_ψ anomalous dimensions $\gamma^{(i)}_\psi$.

$\gamma^{(0)}$	$\gamma^{(1)}$	$\gamma^{(2)}$	$\gamma^{(3)}$
0	44.6667	2177.0737	130 760.2969

TABLE IV. Quenched Z_m anomalous dimensions $\gamma_m^{(i)}$.

$\gamma^{(0)}$	$\gamma^{(1)}$	$\gamma^{(2)}$	$\gamma^{(3)}$
8	252	11 769.5469	557 837.9375

TABLE V. Quenched Z_T anomalous dimensions $\gamma_T^{(i)}$.

$\gamma^{(0)}$	$\gamma^{(1)}$	$\gamma^{(2)}$
2.666 67	80.4444	3268.2996

Figure 11 shows both $\Gamma_A((ap)^2, ma = 0)$ and $\Gamma_A^{\rm SI}((ap)^2, ma = 0)$ as a function of $(pa)^2$. By comparing them, we see that the renormalization group running due to Z_ψ is not appreciable for $(pa)^2 > 3$, but it does tend to make the SI data flatter as a function of $(pa)^2$. The remaining scale dependence of $\Gamma_A^{\rm SI}((ap)^2, ma = 0)$ is very small. A plausible explanation for it is an $(ap)^2$ error [9]. Fitting the remaining scale dependence to the form [9]

$$\Gamma_A^{\rm SI}((ap)^2) = \Gamma_A^{\rm SI} + c(ap)^2, \tag{64}$$

for a range of momenta that is chosen to be "above" the region where the condensate effects are important, one can obtain the scale invariant Γ_A which is denoted as $\Gamma_A^{\rm SI}$.

When a linear fit of the SI data versus $(ap)^2$ is performed for $2.4 < (ap)^2 < 5.7$, the gradient is ≈ 0.001. In the ideal case, the gradient should be zero. This small value is thus interpreted as an $O(a^2)$ error. This shows that the $(pa)^2$ error of the ratio of Z_ψ and Z_A is small, but we do not know their individual $(pa)^2$ error separately. It appears that the $(pa)^2$ error in Z'_ψ as defined from the quark propagator in Eq. (19) is as large as $\sim 10\%$ at $p = 2$ GeV [9,12]. However, this relatively large $(pa)^2$ error in $Z_\psi^{\rm SI}$ must be

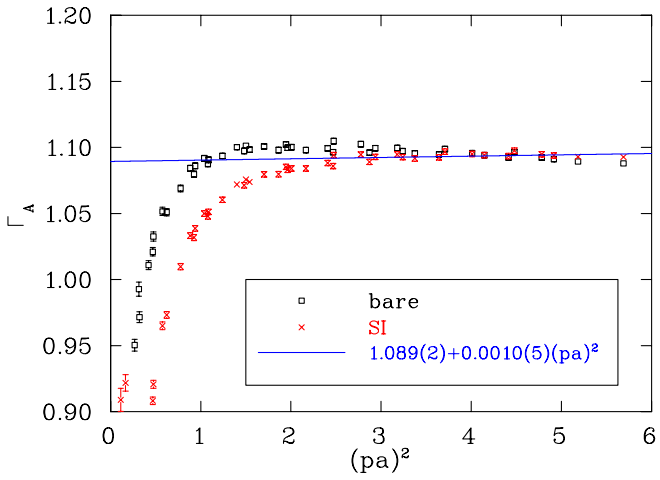

FIG. 11 (color online). Γ_A (labeled as "bare") and the scale invariant $\Gamma_A^{\rm SI}$ versus $(pa)^2$ in the chiral limit. They coincide near $(pa)^2 = 4.1$. The later is almost $(pa)^2$ independent after $(pa)^2 > 2.4$, the slope versus $(pa)^2$ is about 0.001.

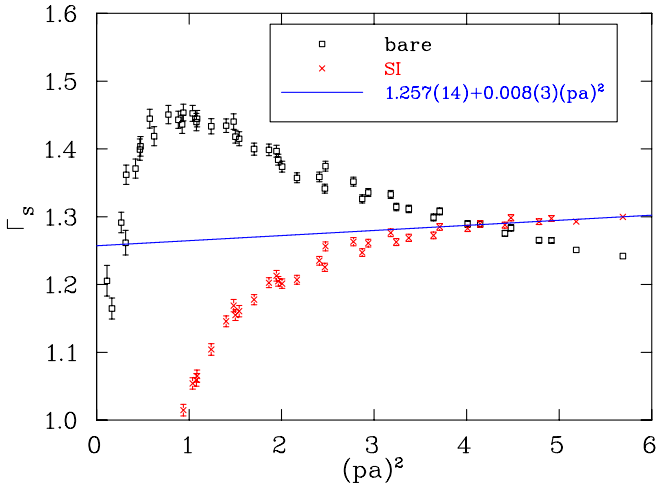

FIG. 12 (color online). The same as Fig. 11 for $\Gamma_S^{\rm sub}$ and $\Gamma_S^{\rm sub,SI}$. The slope of SI versus $(pa)^2$ is about 0.008 beyond $(pa)^2 \geq 4.0$.

cancelled to a large extent by that of Z_A, resulting in a small $(pa)^2$ error in $\Gamma_A^{\rm SI}$ (only 0.4% at $(pa)^2 = 4.1$). As will be discussed in the next subsection, we will use Z_A determined from the chiral Ward identity to obtain Z_ψ. Since Z_A, in this case, is determined from the pion state at rest, it is at a momentum scale of $\Lambda_{\rm QCD}$. Thus, it should have small $(pa)^2$ error. Using this value of Z_A and $\Gamma_A^{\rm SI}((ap)^2, ma = 0)$ to obtain $Z_\psi^{\rm SI}$, and thus $Z_\psi^{RI}(2\ {\rm GeV})$ should give a $(pa)^2$ error of $\sim 0.4\%$ which we shall consider as the systematic error in $O(a^2)$.

In the case of $\Gamma_S^{\rm sub} = Z_\psi/Z_S$, both Z_ψ and Z_S run with μ^2. Figure 12 shows $\Gamma_S^{\rm sub}$ and the corresponding scale invariant (SI) vertex, $\Gamma_S^{\rm sub,SI}$, after three loop running. We see that $\Gamma_S^{\rm sub,SI}$ is much flatter than $\Gamma_S^{\rm sub}$ for $(pa)^2 > 3.0$. The linear fit of the SI data versus $(pa)^2$ in the range of $4.0 < (ap)^2 < 5.7$, gives a gradient of 0.008(3). This is an order of magnitude larger than that of the axial vector (and that of the tensor current below). This relatively larger gradient could be due to the systematic uncertainty in subtracting the chiral divergence in Γ_S or the mismatch of the $(pa)^2$ errors between $Z_\psi^{\rm SI}$ and $Z_S^{\rm SI}$ or both.

The SI result of Γ_T which comes from the three loop running of Z_T [49] and four loop running of Z_ψ is plotted in Fig. 13 along with Γ_T. The linear fit to the SI data in the range of $2.0 < (ap)^2 < 5.7$ gives a gradient of $-0.0004(2)$.

It is worthwhile pointing out that comparing to the Domain-Wall fermion case on a $16^3 \times 32 \times 16$ lattice with Wilson gauge action at $\beta = 6.0$ [9], we find that the remaining scale dependence as measured by the gradient in $(pa)^2$ is comparable for the $\Gamma_S^{\rm SI}$ case. But the gradient for $\Gamma_A^{\rm SI}/\Gamma_T^{\rm SI}$ is 1/2 orders of magnitude smaller than that in the Domain-Wall fermion case. Since the Domain-Wall fermion with finite 5th dimension and the rational polynomial approximation of the sign function that we adopt in the present work are two different approximations of the same

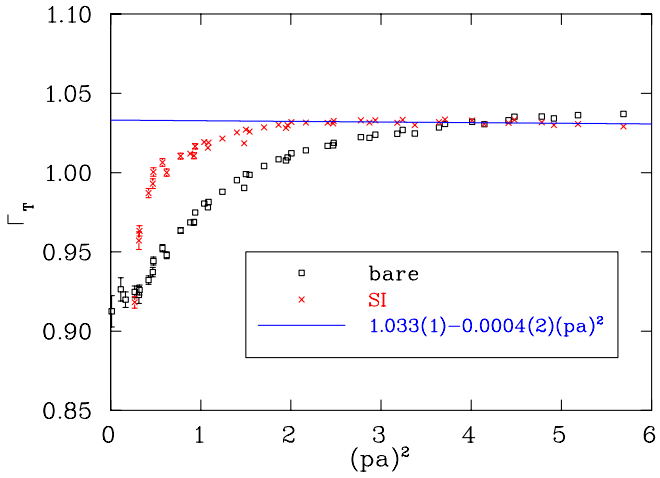

FIG. 13 (color online). The same as Fig. 11 for Γ_T and $\Gamma_T^{\rm SI}$. The later is almost $(pa)^2$ independent after $(pa)^2 > 2.0$, the slope versus $(pa)^2$ is about -0.0004.

overlap fermion in 4 dimensions [53], the $(pa)^2$ errors in the scale invariant vertices serve as a measure of the $O(a^2)$ errors of the approximation.

A. Determining Z_A from Ward identity

Before applying the renormalization group running (an inverse operation of Eq. (63)) to match to the $\overline{\rm MS}$ scheme at certain scale, we need to input Z_A to Eq. (23) in order to determine other renormalization constants from the respective vertex functions. As explained in Sec. II B, we prefer using Z_A from the chiral Ward identity to determine Z_ψ than directly obtaining it from the quark propagator. This is partly due to the fact that there is ambiguity in the lattice definition of momentum [9] in Eq. (19). Furthermore, it is shown in the study with Domain-Wall fermion [9] and an earlier study of the overlap fermion [12] that the $(pa)^2$ errors in the scale invariant $Z_\psi^{\rm SI}$ are quite large.

The renormalization constant Z_A for the axial current $A_\mu = \bar\psi(i\gamma_\mu\gamma_5(1 - D/2\rho)\frac{\tau^a}{2})\psi$ can be obtained directly through the axial Ward identity

$$Z_A \partial_\mu A_\mu = 2Z_m m Z_P P, \tag{65}$$

where $P = \bar\psi(i\gamma_5(1 - D/2\rho)\frac{\tau^a}{2})\psi$ is the pseudoscalar density. For the case of the overlap fermion [11,19,21], $Z_m = Z_S^{-1}$ and $Z_S = Z_P$. Thus, Z_m and Z_P cancel in Eq. (65) and one can determine Z_A to $O(a^2)$ nonperturbatively from the axial Ward identity using the bare mass m and bare operator P. To obtain Z_A, we shall consider the on-shell matrix elements between the vacuum and the zero-momentum pion state for the axial Ward identity

$$Z_A\langle 0|\partial_\mu A_\mu|\pi(\vec p = 0)\rangle = 2m\langle 0|P|\pi(\vec p = 0)\rangle, \tag{66}$$

where the matrix elements can be obtained from the zero-momentum correlators

$$G_{\partial_4 A_4 P}(\vec p = 0, t) = \Big\langle \sum_{\vec x} \partial_4 A_4(x) P(0)\Big\rangle,$$
$$G_{PP}(\vec p = 0, t) = \Big\langle \sum_{\vec x} P(x) P(0)\Big\rangle. \tag{67}$$

The nonperturbative Z_A is then

$$Z_A = \lim_{m\to 0, t\to\infty} \frac{2mG_{PP}(\vec p = 0, t)}{G_{\partial_4 A_4 P}(\vec p = 0, t)}. \tag{68}$$

Given that the time derivative itself in $G_{\partial_4 A_4 P}(\vec p = 0, t)$ invokes an $O(a^2)$ error, it would be better to adopt a definition for Z_A which is devoid of this superfluous $O(a^2)$ error. This can be achieved by noticing that, at large t where the pion state dominates the propagator $G_{\partial_4 A_4 P}(\vec p = 0, t)$, one can effectively make the substitution

$$G_{\partial_4 A_4 P}(\vec p = 0, t) \xrightarrow[t\to\infty]{} m_\pi G_{A_4 P}(\vec p = 0, t). \tag{69}$$

Consequently, Eq. (68) becomes

$$Z_A = \lim_{m\to 0, t\to\infty} \frac{2mG_{PP}(\vec p = 0, t)}{m_\pi G_{A_4 P}(\vec p = 0, t)}. \tag{70}$$

Since the G_{PP} and $G_{A_4 P}$ correlators are calculated at finite ma, we shall define the renormalization factor

$$\tilde Z_A(ma) = \lim_{t\to\infty} \frac{2mG_{PP}(\vec p = 0, t)}{m_\pi G_{A_4 P}(\vec p = 0, t)}, \tag{71}$$

where the massless limit would give Z_A. We plot the results of $\tilde Z_A(ma)$ from Eq. (71) in Fig. 14. In view of the fact that there is no $O(a)$ error with the overlap fermion, $\tilde Z_A(ma)$

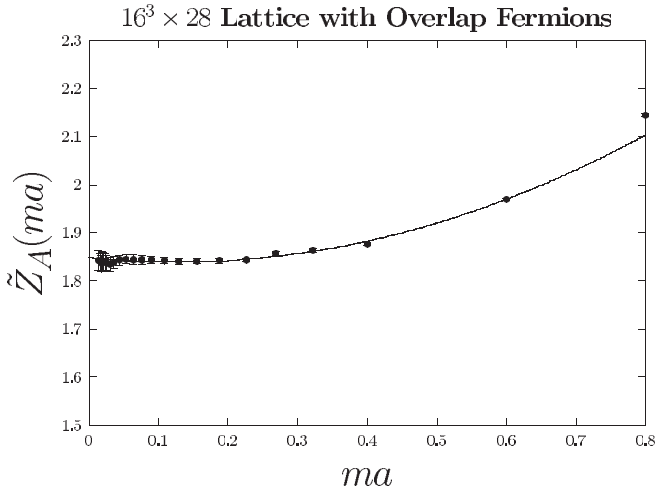

FIG. 14. $\tilde Z_A(ma)$ vs quark mass ma.

could have terms like $m\Lambda_{\rm QCD}a^2$ and m^2a^2, but could also have terms like $m/\Lambda_{\rm QCD}$ and $(m/\Lambda_{\rm QCD})^2$. Thus, we parametrize it with the form which is linear and quadratic in m [17,21]

$$\tilde{Z}_A(ma) = Z_A(1 + b_A m + c_A m^2). \quad (72)$$

As noticed before [21], it is conspicuously flat as a function of ma suggesting that the $O(a^2)$ error from the action and the axial-vector operator is small. From the fitting to the form in Eq. (72) for the range of ma from 0.014 to 0.6, we find that $Z_A = 1.849(4)$, $b_A = -0.347(16)$ (in units of $\Lambda_{\rm QCD}a^2$ with $\Lambda_{\rm QCD} = 0.238$ GeV), and $c_A = 0.317(21)$ (in units of a^2) with $\chi^2/{\rm dof} = 0.54$.

We observe that Z_A is determined to the precision of 0.2% in statistical error. It is thus more desirable [9] to use Z_A from the Ward identity and Γ_A to determine all the other renormalization constants.

From the renormalization condition Eq. (22), we finally obtain $Z_\psi^{\rm SI}$

$$Z_\psi^{\rm SI} = Z_A\Gamma_A^{\rm SI}, \quad (73)$$

and the other SI renormalization constants from Eq. (23)

$$Z_O^{\rm SI} = Z_A\frac{\Gamma_A^{\rm SI}}{\Gamma_O^{\rm SI}}. \quad (74)$$

Since we normalize the scale invariant vertex functions to the RI scheme at $(pa)^2 = 4.1$, the renormalization constant determined in Eq. (74) is just $Z_O^{\rm RI}(\mu = 2\ {\rm GeV})$.

B. Matching to $\overline{\rm MS}$ scheme

In order to confront experiments, one frequently likes to quote the final results in the $\overline{\rm MS}$ scheme at certain scale. For light hadrons, the popular scale is 2 GeV. To obtain the renormalization constants in the $\overline{\rm MS}$ scheme at 2 GeV, one can use the perturbatively computed coefficient functions in Eq. (59) in the $\overline{\rm MS}$ scheme to evolve the scale invariant renormalization constant to the targeted scale, i.e.

$$Z_O^{\overline{\rm MS}}(\mu) = C_O^{\overline{\rm MS}}(\mu)Z_O^{\rm SI}. \quad (75)$$

Alternatively, one can avoid the step of going to the scale invariant quantity and, instead, match directly from the RI scheme to the $\overline{\rm MS}$ scheme at the same scale. The perturbative expansion of the ratio $Z^{\overline{\rm MS}}/Z^{\rm RI}$ to two loop order are given by the finite coefficients in the perturbative expansion of $Z^{\rm RI}$ [20]

$$R = \frac{Z^{\overline{\rm MS}}}{Z^{\rm RI}} = 1 + \frac{\alpha_s}{4\pi}(Z^{\rm RI})_0^{(1)} + \left(\frac{\alpha_s}{4\pi}\right)^2(Z^{\rm RI})_0^{(2)} + \ldots. \quad (76)$$

The numerical values of the matching coefficients, $Z_0^{(1)}$, $Z_0^{(2)}$, and $Z_0^{(3)}$ in Eq. (76) used for Z_ψ, Z_m, and Z_T have been calculated in Ref. [48] and Ref. [54], and are collected in Table VI.

TABLE VI. Quenched RI to $\overline{\rm MS}$ matching coefficients.

$Z_{(0)}$	$Z_0^{(1)}$	$Z_0^{(2)}$	$Z_0^{(3)}$	R at 2 GeV
Z_ψ	0.0000	−25.4642	−1489.9805	0.987 06
Z_m	-5.3333	−149.0402	−5598.9526	0.851 27
Z_T	0.0000	−46.6654	−2067.9753	0.979 09

TABLE VII. Renormalization constants Z in RI, and $\overline{\rm MS}$ schemes at $\mu = 2$ GeV. The renormalization constant in the SI scheme is normalized to be the same as that in the RI scheme at 2 GeV. These renormalization constants are obtained from the lattice with $a = 0.200$ fm.

Z	RI at 2 GeV	$\overline{\rm MS}$ at 2 GeV
Z_A	1.853(9)	1.853(9)
Z_V	1.846(8)	1.846(8)
Z_P	1.571(15)	1.845(17)
Z_S	1.567(13)	1.841(15)
Z_T	1.966(6)	1.925(6)
Z_ψ	2.307(18)	2.277(18)

The results for Z_A, Z_V, Z_P, Z_S, Z_T, and Z_ψ in the RI and $\overline{\rm MS}$ scheme at 2 GeV (for Z_P, Z_S, Z_T, and Z_ψ) are listed in Table VII.

VI. FINITE m DEPENDENCE OF THE RENORMALIZATION FACTORS

As discussed in Sec. III, a nonperturbative renormalization of the heavy-light axial current via the chiral Ward identity and the unequal mass Gell-Mann-Oakes-Renner relation is possible with the overlap fermion at finite ma [17]. This offers an opportunity to calculate heavy-light decay constants and transition matrix elements without being subjected to the uncertainty of the perturbative calculation of the renormalization constants. In this section, we shall examine the finite m behavior of the renormalization factors. This is useful for the future study of heavy-light decays and transitions.

Similar to the renormalization factor $\tilde{Z}_A(ma)$ defined in Eqs. (71) and (72) for the axial current, we shall parametrize the renormalization factor for the other operators by

$$\tilde{Z}_O(ma) = Z_O(\mu a, g(a))(1 + b_O m + c_O m^2), \quad (77)$$

where the linear m term includes terms like $m\Lambda_{\rm QCD}a^2$ and $m/\Lambda_{\rm QCD}$ and the quadratic m term includes terms like m^2a^2 and $(m/\Lambda_{\rm QCD})^2$.

To obtain the renormalization factors for $O = V, S, P, T$, and ψ, we shall adopt the same renormalization condition Eq. (14) for finite m. We shall use the quark propagator to

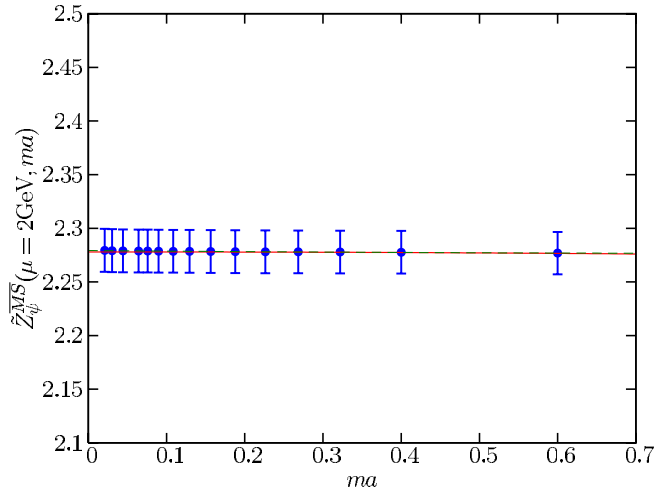

FIG. 15 (color online). Renormalization factor $\tilde{Z}_A(ma)$ against quark mass ma. The solid line is the correlated fit and the dashed line is the uncorrelated fit.

obtain the finite m dependence for $\tilde{Z}_\psi(ma)$ from Eq. (19), except with $Z_\psi = \tilde{Z}_\psi(ma = 0)$ normalized from Z_A via the renormalization condition, Eq. (22). We then follow the above procedure in the preceding sections to obtain $\tilde{Z}_A(ma)$, $\tilde{Z}_V(ma)$, $\tilde{Z}_S(ma)$, $\tilde{Z}_P(ma)$, and $\tilde{Z}_T(ma)$. The $\tilde{Z}_\psi^{\overline{\mathrm{MS}}}(ma, \mu = 2\ \mathrm{GeV})$ for $\tilde{Z}_\psi(ma)$ in the $\overline{\mathrm{MS}}$ scheme at $\mu = 2$ GeV is plotted in Fig. 15. The corresponding results on $\tilde{Z}_A(ma)$, $\tilde{Z}_V(ma)$, $\tilde{Z}_S^{\overline{\mathrm{MS}}}(ma, \mu = 2\ \mathrm{GeV})$, $\tilde{Z}_P^{\overline{\mathrm{MS}}}(ma, \mu = 2\ \mathrm{GeV})$, and $\tilde{Z}_T^{\overline{\mathrm{MS}}}(ma, \mu = 2\ \mathrm{GeV})$ are plotted in Fig. 16, 17, 19, 18, and 20, respectively.

We observe that these curves are all rather flat, with less than 3% deviation for ma as large as 0.6. We make a correlated fit of the finite m behavior with the form in Eq. (77). The coefficients b_O and c_O are listed in Table VIII. The fitted curves are drawn in Figs. 16, 17, 19, 18, and 20 as solid lines. For comparison, we also plot the uncorrelated fits as dashed lines which have much smaller χ^2/dof than those of the correlated fits. The flat-

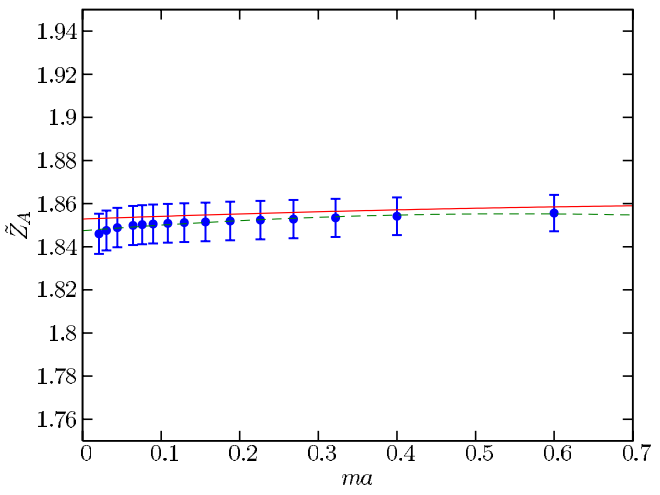

FIG. 16 (color online). Renormalization factor $\tilde{Z}_A(ma)$ calculated from Γ_A against quark mass ma. The solid line is the correlated fit and the dashed line is the uncorrelated fit.

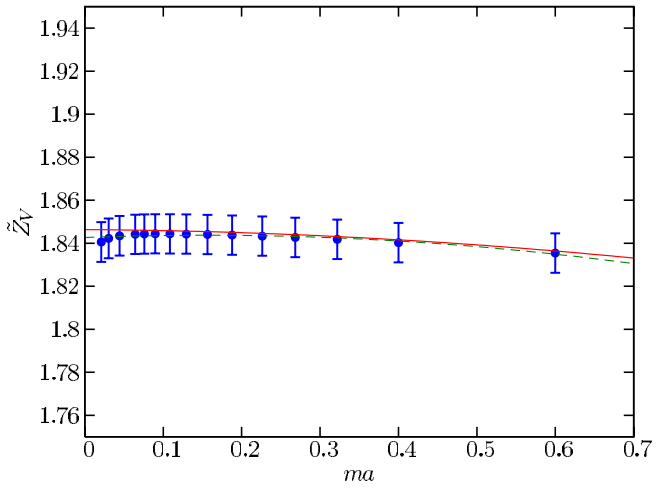

FIG. 17 (color online). The same as in Fig. 16 for $\tilde{Z}_V(ma)$.

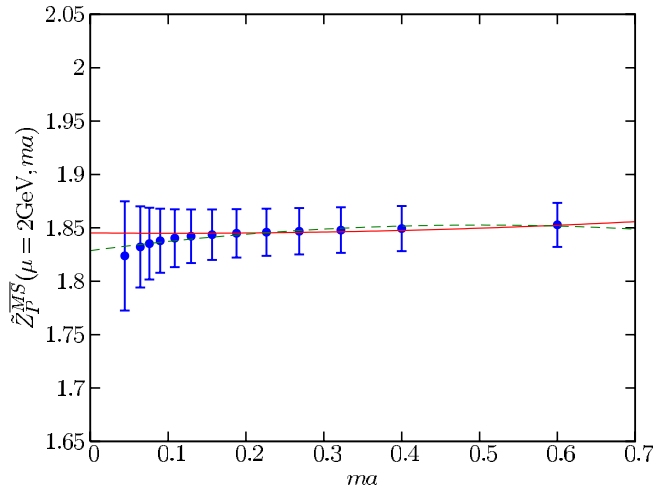

FIG. 18 (color online). The same as in Fig. 16 for the renormalization factor $\tilde{Z}_P{}^{\overline{\mathrm{MS}}}(ma)$ in the $\overline{\mathrm{MS}}$ scheme at $\mu = 2$ GeV.

TABLE VIII. Mass dependence of the renormalization factors as defined in Eq. (77). b_O is in units of $\Lambda_{\mathrm{QCD}} a^2$ with $\Lambda_{\mathrm{QCD}} = 0.238$ GeV. c_O is in units of a^2.

	$Z_O^{\overline{\mathrm{MS}}}$ (2 GeV)	b_O	c_O	χ^2/dof
A	1.853(9)	0.029(16)	−0.003(2)	1.3
V	1.846(8)	−0.0055(33)	−0.013(7)	2.2
P	1.845(20)	−0.015(12)	0.017(4)	0.3
S	1.841(15)	0.22(19)	0.004(2)	0.7
T	1.925(6)	−0.012(8)	−0.015(3)	1.6
ψ	2.277(18)	−0.001(2)	0.002(1)	0.8

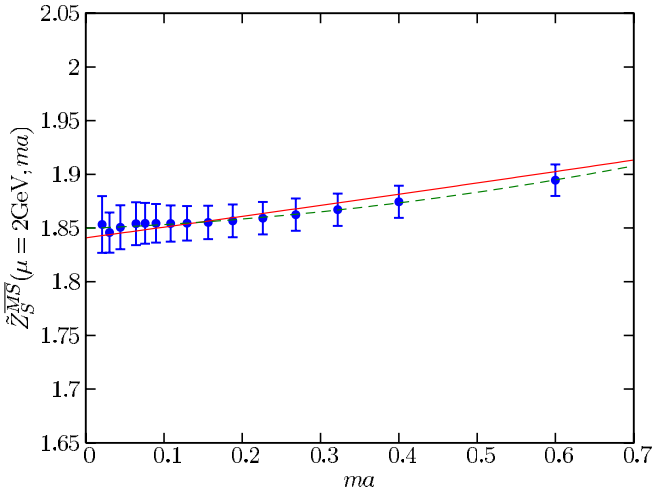

FIG. 19 (color online). The same as in Fig. 18 for $\tilde{Z}_S{}^{\overline{\mathrm{MS}}}(ma)$.

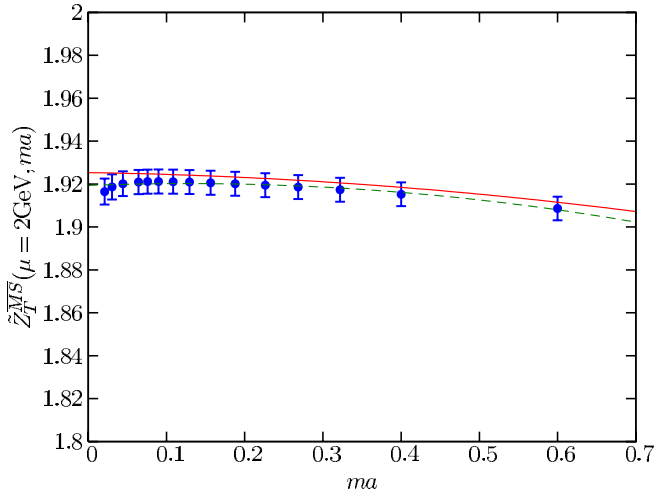

FIG. 20 (color online). The same as in Fig. 18 for $\tilde{Z}_T{}^{\overline{\mathrm{MS}}}(ma)$.

ness in ma suggests that the $O((ma)^2)$ dependence is weak. This is consistent with the findings for the π and ρ masses [19] and their dispersion relations [17]. The observed $O(ma^2)$ and $O(m^2a^2)$ dependence are much weaker than those found with the chirally improved Dirac operator [10]. We do not know the finite m behavior of the domain-wall fermion from the study of the quark bilinear operators [9]. The study of $\tilde{Z}_A(ma)$ and $\tilde{Z}_V(ma)$ from the nucleon matrix elements found much stronger $O(ma^2)$ and $O(m^2a^2)$ dependence than observed here.

We should point out that in Sec. VA, $\tilde{Z}_A(ma)$ was defined in Eqs. (71) and (72) with the implicit assumption that $\tilde{Z}_P(ma)$ is not very different from $\tilde{Z}_S(ma)$ for the available range of ma. Even though this does not in principle affect the extraction of the renormalization constant Z_A at the massless limit of $\tilde{Z}_A(ma)$, where Z_P is equal to Z_S, the extrapolation could have a large uncertainty if $\tilde{Z}_P(ma)$ is very different from $\tilde{Z}_S(ma)$ for the range of ma which is not close to the chiral limit. Thus, it is gratifying to see in Figs. 18 and 19 that the ma behaviors of $\tilde{Z}_P(ma)$ and $\tilde{Z}_S(ma)$ (in the $\overline{\mathrm{MS}}$ scheme at 2 GeV in this case) are very similar. They differ less than 3% for $ma \leq 0.6$. The upshot is that we should take the ma behavior in $\tilde{Z}_A(ma)$ in Fig. 16 as the correct one, instead of that in Fig. 14 as defined in Eq. (71). Any attempt to correct for the negligence of the ma dependence in $\tilde{Z}_P(ma)$ and $\tilde{Z}_S(ma)$ in Eq. (71) and compare with that in $\tilde{Z}_A(ma)$ in Fig. 16 is expected to reflect different finite ma corrections under different renormalization conditions.

VII. SUMMARY AND OUTLOOK

In this work, we performed a nonperturbative renormalization calculation of the composite quark bilinear operators with the overlap fermion in the regularization-independent scheme from the quark vertex function with high virtuality. The renormalization group running of the renormalization constants were calculated to obtain the scale invariant (SI) renormalization constants and also matched to the $\overline{\mathrm{MS}}$ scheme at $\mu = 2$ GeV. The scale invariant Z_A from the Ward identity and the axial vertex function were used to eliminate the wave function renormalization Z_ψ and determine the renormalization constants from other vertex functions. Since Z_A, as obtained from the Ward identity, has a very small error ($\sim 0.2\%$), it is more desirable to use it to determine Z_ψ instead of using the quark propagator to determine it. The latter can introduce an error as large as $\sim$10%-20% [9].

After subtracting the quenched chiral log divergences in the vertex functions Γ_P and Γ_S due to the presence of the pseudoscalar meson, the expected relation $Z_S = Z_P$ due to chiral symmetry holds to high precision ($\sim 1\%$) for a large range of $(pa)^2$ with $(pa)^2 > 3$. The same is true for the relation $Z_A = Z_V$. The resultant check on the chiral-symmetry relations are comparable to those of the domain-wall fermion [9] and somewhat better than the chirally improved fermion [10] where it is found that $Z_A/Z_V \sim 1.03$ and $Z_P/Z_S \sim 0.95$ for their smallest lattice spacing at $a = 0.078$ fm.

We studied the finite m behavior in the renormalization factors of these composite operators. This is useful if one wants to use the same overlap-Dirac operator for both the light and heavy quarks. With presentday computers, it is not practical to reach a lattice spacing such that $ma \ll 1$ for the charm and bottom quarks. As such, one would like to have a Dirac operator which has chiral symmetry and, at the same time, has small $O(ma^2)$ and $O(m^2a^2)$ errors. It is suggested [17] that the overlap fermion with its effective quark propagator having the continuum form might be suitable for this purpose. Indeed the $O(ma^2)$ and $O(m^2a^2)$ errors in the dispersion relation are shown to be small [17]. In this study, we find that the finite m dependence is quite gentle in $\tilde{Z}_\psi(ma)$, $\tilde{Z}_A(ma)$, $\tilde{Z}_V(ma)$, $\tilde{Z}_P(ma)$, $\tilde{Z}_S(ma)$, and $\tilde{Z}_T(ma)$. For ma as large as 0.6, the deviations

are generally less than 3.5% in these renormalization factors we studied.

Since the lattice community is geared to carrying out large scale dynamical fermion calculations with chiral fermions, it is worth studying the $(pa)^2$ errors in the scale invariant vertices to gauge the $O(a^2)$ errors and also the mass dependence of the renormalization factors with the overlap fermion.

ACKNOWLEDGMENTS

Support for this research from the Australian Research Council and DOE Grants No. DE-FG05-84ER40154 and No. DE-FG02-02ER45967 and NNSF of China Grant No. 10235040 are gratefully acknowledged.

[1] G. Martinelli, C. Pittori, C. T. Sachrajda, M. Testa, and A. Vladikas, Nucl. Phys. **B445**, 81 (1995).
[2] M. Ciuchini, E. Franco, G. Martinelli, L. Reina, and L. Silvestrini, Z. Phys. C **68**, 239 (1995).
[3] G. Martinelli, S. Petrarca, C. T. Sachrajda, and A. Vladikas, Phys. Lett. B **311**, 241 (1993); **317**, 660(E) (1993).
[4] V. Gimenez, L. Giusti, F. Rapuano, and M. Talevi, Nucl. Phys. **B531**, 429 (1998).
[5] A. Donini, V. Gimenez, G. Martinelli, M. Talevi, and A. Vladikas, Eur. Phys. J. C **10**, 121 (1999).
[6] V. Gimenez, L. Giusti, F. Rapuano, M. Talevi, and A. Vladikas, Nucl. Phys. B, Proc. Suppl. **73**, 210 (1999).
[7] D. Becirevic *et al.*, Phys. Lett. B **444**, 401 (1998).
[8] S. Aoki *et al.* (JLQCD Collaboration), Nucl. Phys. B, Proc. Suppl. **73**, 279 (1999).
[9] T. Blum, N. Christ, C. Cristian, C. Dawson, G. Fleming, G. Liu, R. Mawhinney, A. Soni, P. Vranas, M. Wingate, L. Wu, and Y. Zhestkov, Phys. Rev. D **66**, 014504 (2002).
[10] C. Gattringer, M. Göckeler, P. Huber, and C. B. Lang, Nucl. Phys. **B694**, 170 (2004).
[11] L. Giusti, C. Hoelbling, and C. Rebbi, Phys. Rev. D **64**, 114508 (2001); **65**, 079903(E) (2002).
[12] J. B. Zhang, D. B. Leinweber, K. F. Liu, and A. G. Williams, Nucl. Phys. B, Proc. Suppl. **128**, 240 (2004).
[13] R. Narayanan and H. Neuberger, Phys. Lett. B **302**, 62 1993); Nucl. Phys. **B443**, 305 (1995).
[14] H. Neuberger, Phys. Lett. B **417**, 141 (1998); Phys. Lett. B **427**, 353 (1998).
[15] M. Lüscher, Phys. Lett. B **428**, 342 (1998).
[16] R. G. Edwards, U. M. Heller, and R. Narayanan, Phys. Rev. D **59**, 094510 (1999).
[17] K. F. Liu and S. J. Dong, hep-lat/0206002 [Int. Jour. Mod. Phys. A (to be published)].
[18] H. Neuberger, Nucl. Phys. B, Proc. Suppl. **83**, 67 (2000).
[19] S. J. Dong, F. X. Lee, K. F. Liu, and J. B. Zhang, Phys. Rev. Lett. **85**, 5051 (2000).
[20] E. Franco and V. Lubicz, Nucl. Phys. **B531**, 641 (1998).
[21] S. J. Dong, T. Draper, I. Horváth, F. X. Lee, K. F. Liu, and J. B. Zhang, Phys. Rev. D **65**, 054507 (2002).
[22] P. H. Ginsparg and K. G. Wilson, Phys. Rev. D **25**, 2649 (1982).
[23] P. Hasenfratz *et al.*, Nucl. Phys. **B643**, 280 (2002).
[24] Y. Kikukawa and A. Yamada, Nucl. Phys. **B547**, 413 (1999).
[25] T. W. Chiu and S. Zenkin, Phys. Rev. D **59**, 074501 (1999).
[26] H. Neuberger, Phys. Rev. D **57**, 5417 (1998).
[27] T. W. Chiu, Phys. Rev. D **60**, 034503 (1999).
[28] S. Capitani, M. Goeckeler, R. Horsley, P. E. L. Rakow, and G. Schierholz, Phys. Lett. B **468**, 150 (1999).
[29] F. D. R. Bonnet, P. O. Bowman, D. B. Leinweber, A. G. Williams, and J. B. Zhang, Phys. Rev. D **65**, 114503 (2002).
[30] S. Tamhankar, A. Alexandru, Y. Chen, S. J. Dong, T. Draper, I. Horvath, F. X. Lee, K. F. Liu, N. Mathur, and J. B. Zhang, hep-lat/0507027.
[31] Y. Chen, S. J. Dong, T. Draper, I. Horváth, F. X. Lee, K. F. Liu, N. Mathur, and J. B. Zhang, Phys. Rev. D **70**, 034502 (2004).
[32] M. Golterman, Y. Shamir, and B. Svetitsky, Phys. Rev. D **72**, 034501 (2005).
[33] T. Draper, N. Mathur, J. B. Zhang, A. Alexandru, Y. Chen, S. J. Dong, I. Horvath, F. X. Lee, and S. Tamhankar, hep-lat/0510075.
[34] P. Hernandez, K. Jansen, and M. Lüscher, Nucl. Phys. **B552**, 363 (1999).
[35] A. Cucchieri and T. Mendes, Phys. Rev. D **57**, R3822 (1998).
[36] F. D. R. Bonnet, P. O. Bowman, D. B. Leinweber, A. G. Williams, and D. G. Richards, Aust. J. Phys. **52**, 939 (1999).
[37] L. Giusti, S. Petrarca, B. Taglienti, and N. Tantalo, Nucl. Phys. B, Proc. Suppl. **119**, 962 (2003).
[38] J. van den Eshof *et al.*, Comput. Phys. Commun. **146**, 203 (2002); Nucl. Phys. B, Proc. Suppl. **106**, 1070 (2002).
[39] M. Bochicchio, L. Maiani, G. Martinelli, G. C. Rossi, and M. Testa, Nucl. Phys. **B262**, 331 (1985).
[40] P. Hasenfratz, Nucl. Phys. **B525**, 401 (1998).
[41] C. Alexandrou, E. Follana, H. Panagopoulos, and E. Vicari, Nucl. Phys. **B580**, 394 (2000).
[42] K. Lane, Phys. Rev. D **10**, 2605 (1974); H. D. Politzer, Nucl. Phys. **B117**, 397 (1976); P. Pascual and E. de Rafael, Z. Phys. C **12**, 127 (1982).
[43] D. Becirevic, V. Gimenez, V. Lubicz, and G. Martinelli, Phys. Rev. D **61**, 114507 (2000).
[44] S. Sharpe, Phys. Rev. D **46**, 3146 (1992).
[45] L. Giusti and A. Vladikas, Phys. Lett. B **488**, 303 (2000).
[46] N. Mathur, Y. Chen, S. J. Dong, T. Draper, I. Horváth, F. X. Lee, K. F. Liu, and J. B. Zhang, Phys. Lett. B **605**, 137 (2005).

[47] L. Del Debbio, L. Giusti, and C. Pica, Phys. Rev. Lett. **94**, 032003 (2005).
[48] K. G. Chetyrkin and A. Retey, Nucl. Phys. **B583**, 3 (2000).
[49] J. A. Gracey, Nucl. Phys. **B667**, 242 (2003).
[50] Aleksey I. Alekseev, Few-Body Syst. **32**, 193 (2003).
[51] T. van Ritbergen, J. A. M. Vermaseren, and S. A. Larin, Phys. Lett. B **400**, 379 (1997).
[52] S. Capitani, M. Lüscher, R. Sommer, and H. Wittig (ALPHA), Nucl. Phys. **B544**, 669 (1999).
[53] R. C. Brower, H. Neff, and K. Orginos, Nucl. Phys. B, Proc. Suppl. **140**, 686 (2005).
[54] J. A. Gracey, Nucl. Phys. **B662**, 247 (2003).